# THE EFFECTS OF WING MANIPULATION ON AUTOMATED CUTTING OF BIOLOGICAL MATERIALS

A Thesis
Presented to
The Academic Faculty

By

Mark R. Claffee

In Partial Fulfillment
Of the Requirements for the Degree
Master of Science in Mechanical Engineering

Georgia Institute of Technology

August 2006

**THE EFFECTS OF WING MANIPULATION ON AUTOMATED CUTTING OF BIOLOGICAL MATERIALS**

Approved by:

Dr. Kok-Meng Lee, Advisor
The George W. Woodruff
School of Mechanical Engineering
*Georgia Institute of Technology*

Dr. Shreyes N. Melkote
The George W. Woodruff
School of Mechanical Engineering
*Georgia Institute of Technology*

Dr. Daniel Fletcher
Department of Poultry Science
*University of Georgia*

Date Approved: June 28, 2006

## ACKNOWLEDGEMENTS

This work was made possible by contributions, support, and guidance from my advisor, Dr. Kok-Meng Lee. Dr. Lee encouraged me to always clearly think through and define my research before trying to tackle complicated problems. His guidance allowed me to further develop skills that will forever be useful in whichever career path I choose. I would also like to thank my thesis committee members, Dr. Shreyes N. Melkote and Dr. Daniel Fletcher, for their interest in my topic and their time and effort in reviewing this thesis.

In addition, I received much support from my supervisor at the Georgia Tech Research Institute, Gary McMurray. His leadership of the Intelligent Cutting project allowed me to learn the skills necessary to narrow down and solve broad ranging problems. My fellow researcher, Debao Zhou, gave many hours of his time in help determining and refining which path my research should follow. The remainder of the staff at the Georgia Tech Research Institute was always willing to help with the set-up and development of hardware as well as providing a sounding board for several of my ideas.

I would like to thank my parents and sister for the endless support they gave every step of the way. Also, thank you to my late great-uncle, James A. Holmes, who made it possible for me to follow any educational path.

Funding for this research has been provided by the Agricultural Technology Research Program (N4410.520 and N4410.620) through the Georgia Tech. Research Institute. Chicken broilers and front halves were supplied by Tyson Foods, Inc.

## TABLE OF CONTENTS

## LIST OF TABLES

## LIST OF FIGURES

## NOMENCLATURE

### Capital Letters

| | |
|---|---|
| $A$ | Ligament cross-sectional area |
| $C_o$ | Ligament mechanics scaling coefficient |
| $F_o$ | Theoretical ligament tensile force |
| $F_x$ | Manipulation for in $x_m$ direction |
| $F_y$ | Manipulation for in $y_m$ direction |
| $F_z$ | Manipulation for in $z_m$ direction |
| $H$ | Horizontal cutting force |
| $K$ | Cutting force |
| $\vec{L}_{jh}$ | $j^{th}$ ligament to humerus attachment point vector in C-frame |
| $\vec{L}_{jc}$ | $j^{th}$ ligament to coracoid attachment point vector in C-frame |
| $\vec{L}_{jh}^{free}$ | $j^{th}$ non-manipulated humerus attachment point vector in C-frame |
| $\vec{O}_c$ | Origin of inertial frame $X_C Y_C Z_C$ |
| $\vec{O}_f$ | Origin of f-frame |
| $R$ | Material fracture toughness |
| $\lfloor R_{mf} \rfloor$ | Rotation transformation matrix from f-frame to m-frame |
| $[R_{mc}]$ | Rotation transformation matrix from C-frame to m-frame |
| $\lfloor \hat{R}_{mf} \rfloor$ | Coordinate transformation matrix from f-frame to m-frame |
| $\lfloor \hat{R}_{cm} \rfloor$ | Coordinate transformation matrix from m-frame to C-frame |

$\vec{T}_j$ $j^{th}$ ligament tension vector

$V$ Vertical cutting force

**Lower Case Letters**

$a$ Crack propagation displacement

$a_1$ Linear coefficient of biological material force vs. displacement characteristic

$a_2$ Quadratic coefficient of biological material force vs. displacement characteristic

$\vec{f}_m$ Manipulation force vector in m-frame

$h$ Displacement of cutting in the horizontal direction

$k$ Displacement of cutting in direction of cutting force

$\vec{\ell}_{jh}$ $j^{th}$ ligament to humerus attachment point vector in m-frame

$\vec{m}_m$ Manipulation moment vector in m-frame

$m_o$ Ligament mechanics exponent

$\vec{u}_j$ $j^{th}$ ligament direction unit vector

$v$ Displacement of cutting in the vertical direction

$w$ Cut width

**Greek Letters**

$\delta$ Pull manipulation

$\Delta_j$ $j^{th}$ ligament stretch

$\theta_X$ Rotation of humerus about $X_C$ in relaxed position

$\theta_Y$ Rotation of humerus about $Y_C$ in relaxed position

$\theta_Z$ Rotation of humerus about $Z_C$ in relaxed position

$\vec{\rho}_j$ $j^{th}$ ligament attachment point vector from $O_m$ in C-frame

$\xi$ Slice-Push ratio

$\phi$ Twist manipulation

**Subscripts**

c C coordinate frame

f f coordinate frame

jh $j^{th}$ ligament humerus attachment point

jc $j^{th}$ ligament coracoid attachment point

m m coordinate frame

o Coordiante origin

x, y, z Directions in m-frame

## SUMMARY

Many surgical operations and processing of natural product (such as chicken meat) require accurate presentation of the target area in order to achieve more precise incisions. An excellent example is the deboning automation for chicken breast meat, for which the pose of the wing can greatly affect the cutting efficiency, ability to fixture the object for subsequent operations, and product quality and yield. In contrast to engineering objects, biological products present difficulties such as variation in size, shape, and material properties. Unlike past research, which generally found ways to emulate the cutting motion that is used by the workers, this thesis investigates the effects of wing manipulation on cutting tasks.

The objective of this thesis is to develop an analytical model for characterizing the manipulation for pose presentation of a musculoskeletal structure for a specified incision. The manipulation model consists of joint kinematics, the mechanics of bio-materials, and a grasping mechanism to determine the joint pose and forces for a given manipulation trajectory. The model provides a basis for monitoring the cutting of bio-material via non-visual information, as well as for design of a compliant mechanism that can be used in an industrial automation application. To gain a better understanding, a wing manipulation test-bed consisting of a force/torque sensor at the point of wing manipulation has been developed. To set limits surrounding the research, two specific examples are investigated. The first is needle insertion into bio-materials, and the other is the shoulder cutting operation associated with chicken breast meat deboning. The effects of manipulation on needle insertion forces are used to quantify improvements in insertion

point accuracy and required insertion force. Force signatures are also developed for insertion into the tissues located within the shoulder joint. The shoulder cutting operation requires the development of manipulation and cutting trajectories based on information provided from the model and cutting experimentation. The information gathered from both the manipulation model and needle insertion experiments provide a basis for successful implementation of the automation of the shoulder cut.

While the experimentation presented in this thesis is developed in the context of poultry processing, which has immediate contributions as a tool that would facilitate the design of the automated cutting mechanisms in poultry industry, we expect that the development of the models will find a broad range of applications ranging from general meat processing, to surgical simulation, and physical therapy.

# CHAPTER 1: INTRODUCTION

## 1.1 Introduction

The modeling of biological materials and systems has been an area of increasing interest for the past two decades due to advances in biomedical and the growing needs to automate the processing of natural product (such as meat, fish, and poultry). The development of realistic surgical simulators and training systems has driven the creation of models that can accurately describe the forces present in tool and biological system interaction. Currently, these models have been implemented in haptic feedback training aides as well as basic surgical planning tools. In the food processing industry, the application of biological models will assist in the development of highly automated processing lines. These simulators have never accounted for the effects of manipulation on cutting tasks.

A critical action performed by surgeons during many procedures is the manipulation of the organ and surrounding biological structures. The manipulation of these objects allows for proper presentation to the surgeon, and fixes the structure for subsequent operations. There has been very little research performed regarding the manipulation mechanics of biological systems or the effects of manipulation on common surgical tasks.

This thesis continues to improve upon the automation of the deboning process through experimental investigation into the effects of manipulation of biological structures on probing and cutting tasks. It is common knowledge that cutting on a soft

surface increases the force required as well as decreases the accuracy of the cut. Without a solid backing the material being cut can easily deform resulting in significantly altered orientation and location. In order to eliminate the possibility for deformation the structure needs to be rigidly fixed. This can be accomplished by proper manipulation of the joint.

In the case of the chicken breast meat deboning operation a sequence of cuts are used to allow for the removal of the breast meat and wings from the chicken carcass. During the first cut, a cut around the shoulder, the ligaments connecting the wing to the body around the shoulder need to be cut. Under manipulation of the wing the ligaments can be placed in tension as well as presented in such a manner as to facilitate the automation of this cut. The automation of front half deboning requires the development of simple yet effective cutting and manipulation trajectories. The simplicity of the actions are required due to the requirements imposed by the plant operation. First, the automation line must maintain that same throughput as the manual cutters. This requires the complete cutting of 120 – 180 birds per minute. The system must also increase or maintain product yield. Yield is defined as the weight of the removed butterfly divided by the original front half weight. A small decrease in yield would provide enough loss in product to make the automation line not cost effective. The final implementation must consider the ability of the automating the cutting path and manipulation to meet high requirements.

The work presented in this thesis deals with the development of a ligament based joint manipulation model, a study of the advantages of manipulation during needle

insertion tasks, and the application of a shoulder and cutting tool manipulation to the automation of a biological cutting operation.

## 1.2 Prior Work

The intelligent cutting research project has been underway for several years and has been investigated through various methodologies. In an effort to develop a solid understanding of the task of automating the front half deboning operation in poultry processing plants, several areas have required investigation. Automation via the mimicking of manual cutting paths resulted in complex cutting trajectories which could not be easily modified to accommodate variation in sizes. Also, the use of a six degree-of-freedom (DOF) robot is required to achieve the dexterity required to perform the manual cutting path. Further investigation into the cutting operation proved that knowledge of the location of internal structure such as bones would provide a basis for the development of a less complicated cutting path.

Often in industry, when precision cutting is required, there is well developed and understood theory characterizing the cutting task. Objects are fixed and constrained so to eliminate movement of the material during the cutting operation. This fixing allows for precise knowledge of the location and orientation of the work piece, thus allowing for accurate cuts. However, in areas dealing with biological structures, such as surgery or food processing, the fixing of the structure does not provide enough constraint to provide precise knowledge of the structure location and orientation. Locating the internal structure began the current research direction leading to a simplified cutting path which

utilized external input to the wing and shoulder to restrain, and locate the shoulder structure.

Interest to develop an automated chicken breast meat deboning system has motivated Daley, *et al*. [1999] at Georgia Tech to determine the location of the shoulder bone structure and to simulate manual cutting operations of deboning. Sandlin [1998] combined the use of X-Ray images and machine vision techniques to locate the shoulder bone structure relative to the meat surface. Motivated by the need to understand the cause of cumulative trauma disorder due to repetitive motion, He [2000] employed a combination of machine vision techniques with six-DOF force/torque sensing to track the knife motion of a typical deboning worker and the cutting force. These studies offered some intuitive insights to how human operators perform repetitive cutting at high-speeds. Attempts to duplicate cutting motion of a human operator have been found to be very challenging due to the need to satisfy both accuracy and throughput requirements. Based on the studies of several different cutting paths, Lee [2001] proposed a two cut model for mechanical deboning of chicken breast meat to improve the initial incisions that aim at cutting the three ligaments that attached the wing to the carcass. The cuts were to be performed by a pre-program mechanical cutter. Since then, many different incision methods have been suggested; among these is a custom designed cylindrical (plunger) knife proposed in Holmes, *et al.* [2005]. The performance of the plunger cutter was compared against two previous mentioned cutting paths: The first, referred here as 'Zorro', has been based on a path commonly used by a typical human operator in a poultry processing plant [Daley, 1999]. The second cutting path, called 'Slice and Dice' was designed to simplify the path for implementation by a pre-programmed machine

[Lee, 2001]. A study to develop the basic cutting path was performed prior to directly compare various cutting methods that had been researched individually during the past decade. Three cutting paths (the 'Zorro' and 'Slice and Dice' and a plunger type cutter) were tested manually and the yields recorded to determine the basis for an automatable cutting path. Detailed results can be found in Holmes, *et al.* [2005]. The 'Zorro' cutting path utilizes a standard surgical blade and is similar to the dynamic path performed by manual cutters in the plants. The 'Slice and Dice' cut also utilizes a surgical blade but performs a horizontal cut across the shoulder and then a secondary cut to cut down the scapula. The plunger cutter is a sharpened cylinder the same diameter as the top of the coracoid. The cylinder is located above the shoulder joint and plunged into the meat. The shape and velocity of the cutter is meant to sever the three shoulder ligaments. Three cuts were made using each cutting idea and the yield and loss were determined. Figure 1.1 shows the location of meat left on the carcass for each test.

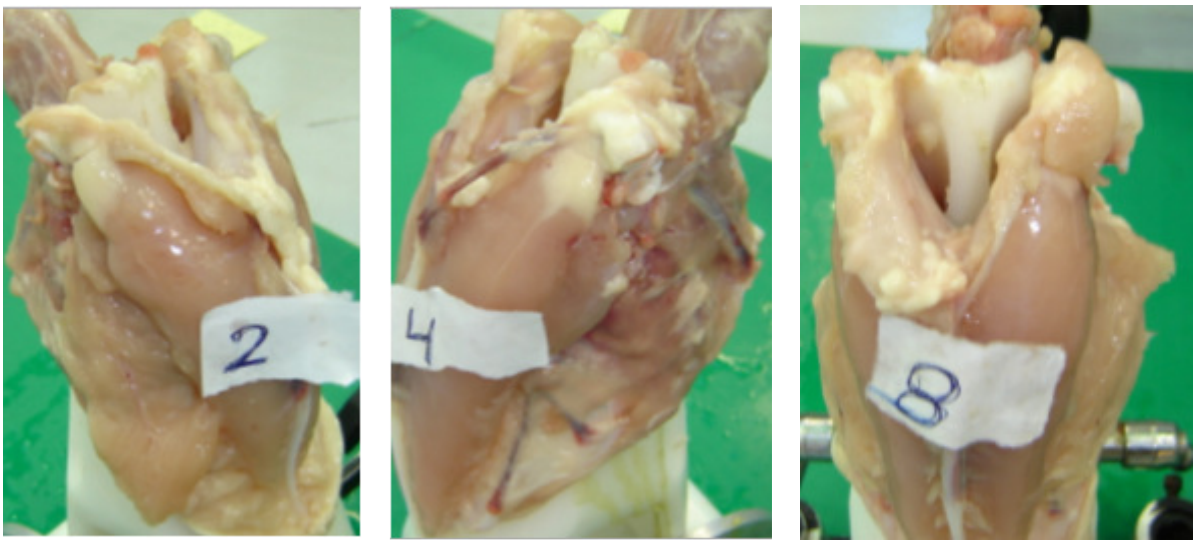


(a) Zorro (b) Slice and Dice (c) Plunger

Figure 1.1: Cutting Comparison Results

The results of the cutting study shows that the average percentage losses for 'Zorro', 'Slice and Dice', and the Plunger are 2.8%, 0.8%, and 4.9% respectively. Figure 1.1 clearly shows a significant amount of meat left along the rib cage during the 'Zorro' cut, as well as on the clavicle and above the coracoid for the 'Plunger'. These results provided sufficient information that the horizontal cutting path performed during the 'Slice and Dice' cut is the path upon which further research in automating the shoulder cut should be focused. The results comparing the three cutting methods have been encouraging, and suggest that the two-cut model can be a practical basis for designing an automated deboning system. Prior attempts to use pin insertion with X-ray images of the bird shoulder joint has led Lee [2005] to investigate the use of pin insertion to obtain force signatures of different material to characterize the shoulder joint to aid in cutting operations. In addition it was experimentally observed that cutting by compression with low-speed slicing is ineffective for cutting highly ductile biomaterials such as meat, which has led Lee [2005] to suggest the use of a high-speed rotational cutter.

## 1.3 Related Research

In this section, several areas of research and application pertaining to biological mechanics, needle insertion, and biological material cutting related to this thesis are examined. Further research, however, is needed in the following areas; (1) the method of manipulating the wing for proper presentation of the cut, (2) the need to locate the three ligaments fort the two-cut incision, and (3) the method to efficiently execute the cut.

### 1.3.1 Biological Material Properties

The understanding of the mechanical properties of biological materials is necessary in fields ranging from meat processing to surgical simulation and medical rehabilitation. Relevant to this thesis is the development of an understanding of ligaments and their properties. Holister in his lecture on the structure and function of ligaments and tendons at the University of Michigan explains the structure of ligaments, and a basis for their properties. He describes the structure as a hierarchy as show in Figure 1.2. He also describes the behavior of ligaments as highly non-linear due to the presence of non-linear elasticity, viscoelasticity, and stress relaxation exhibited in all biological materials. Hansen, *et al.* [2002] proposed a method of experimentally determining the stress/strain properties of a ligament. They claim that due to the structure of biological materials, studies of the structure-function are often difficult or impossible. They study the force response due to stretching of rat tail fascicles. They conclude that the toe-in region of the force response is due to the straightening of the crimps, and the remaining regions are due to the stretching of the fibril and components.

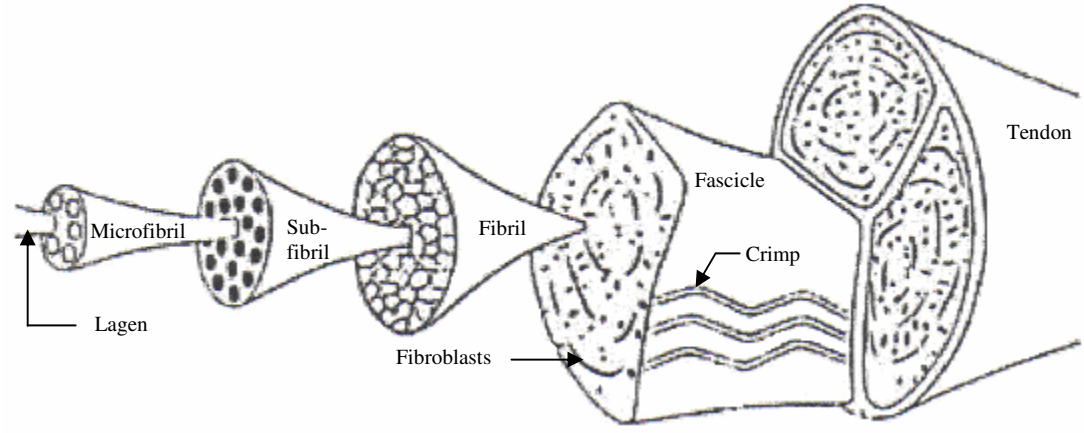


Figure 1.2: Ligament Structure [Holister]

Ligaments are the connective tissues responsible for maintaining skeletal structure and providing joint support. An example of the ligaments found in the human shoulder can be seen in Figure 1.3. Similarly, every joint in animals with internal skeletons are connected and supported by similar ligament structure.

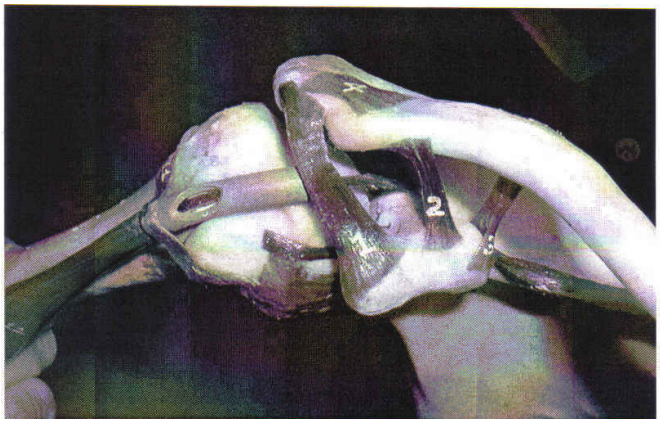

Figure 1.3: Human Shoulder Bones and Ligaments [Lee, 2000]

1.3.2 Needle Insertion

Needle insertion is a crucial action in several medical procedures. Typical procedures include prostate brachytherapy, catheter insertion, tissue biopsy, and several other minimally invasive procedures. Currently, the development of needle insertion models is primarily for the implementation in surgical simulators, surgical planning, and training aides. Kwon, *et al.* [2001] proposes a scheme to model realistic force reflection in spine biopsy needle insertions. Heverly and Dupont [2005] model the needle insertion forces in an effort to develop optimal insertion trajectories for use in image-guided fetal cardiac intervention procedures. Okamura, *et al.* [2004] presents a model of the needle and tissue interaction for the use in realistic surgical simulation and preoperative planning. They note that the gathering of data from biological material is difficult due to the tissues deformation, inhomogeniety, and opacity. Their results show a large

variability of material properties due to inhomogeneity of biological materials and thus a model capable of predicting needle insertion forces every time is impossible to develop. DiMaio and Salcudean [2003] also models the needle insertion, but they focus on the distribution of forces applied along the entire needle. Of importance to this thesis they find that the identification of biological material parameters can be obtained by loading of small tissue samples. Their work also shows significant displacement of a non-fixed biological material upon insertion of the needle resulting in the needle missing a target point, as seen in Figure 1.4. This deformation of the material as well as the difficulties involved in modeling the process of motivated us to develop a method to improve placement accuracy of needle insertion and to predict the required force due to manipulation of the limb or surrounding tissues.

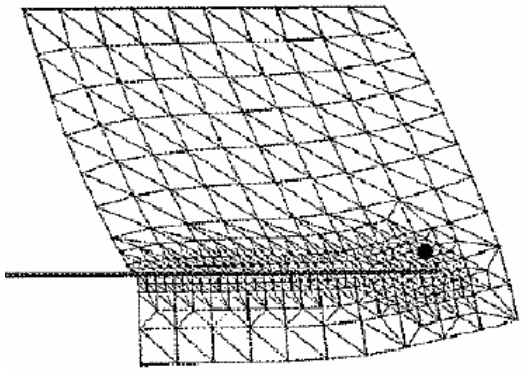

Figure 1.4: Needle Insertion to Target Point [DiMaio, 2003]

### 1.3.3 Cutting Biological Material

In developing applications for limb manipulation, it is clear that a combination of manipulation and cutting has eased manual cutting tasks and can potentially improve the performance of industrial automated cutting. In order to determine the proper manipulation, the mechanics of cutting must first be understood. Atkins and Jeronimidis

[2004] study the effect of "pressing and slicing" on the cutting of biological materials. They present data based on the fracture toughness of the biomaterial, supporting the commonly held notion that slicing or sawing motion will allow for smaller cutting forces. Through the development of a slice-push ratio, $\xi$, the normalized required cutting forces in the compression and slicing directions can be predicted. The addition of even the smallest slicing action results in a significant decrease in compression forces during cutting as seen in Figure 1.5.

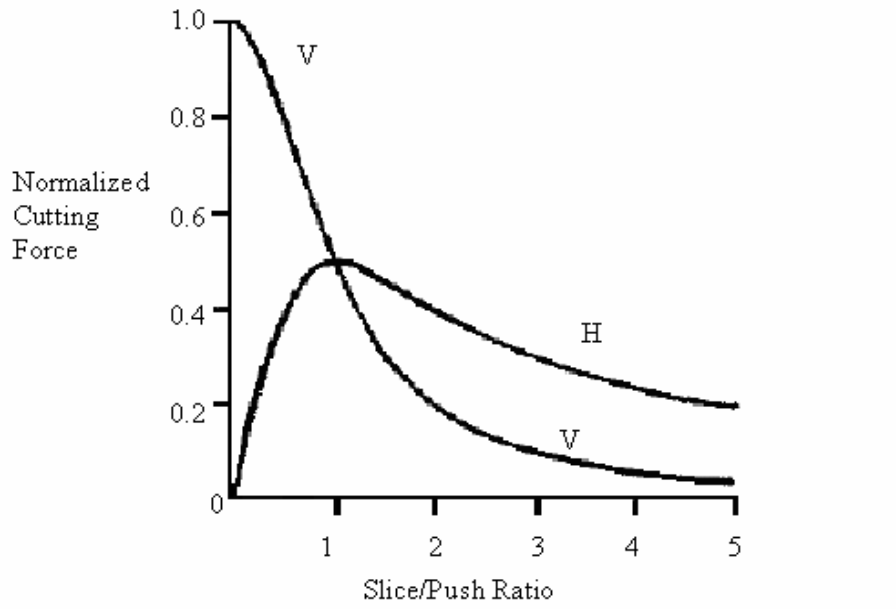


Figure 1.5: Variation of Normalized Forces for Frictionless Orthogonal Cutting [Atkins, 2004]

Similarly, Mahvash and Hayward [2001] present the cutting of deformable materials as a sequence of events. First, the body deforms without cutting occurring, then rupture of the material occurs along the cutting edge, and lastly, the continuation of the cut work is spent in separating the material as well as overcoming the fracture toughness.

The understanding of the cutting of biological materials has been investigated in areas well outside the field of medicine or food processing. In a study of the form and function of predator teeth, Frazzetta [1988], discusses the physics of cutting compliant substrates, and offers a preliminary approach intended to guide research on sharks and other predatory groups. He scans the implications of various tooth designs on puncture and cutting of prey flesh.

## 1.4 Problem Description

This section presents an overview of the current poultry processing operation as well as a more detailed understanding of the area of deboning. The deboning process is where the application of the work presented in this thesis will occur. These tasks are outlined in Figure 1.6.

### 1.4.1 Current Poultry Processing Operation

Poultry processing plants perform several tasks in the processing of live product to the packaging of finished products.

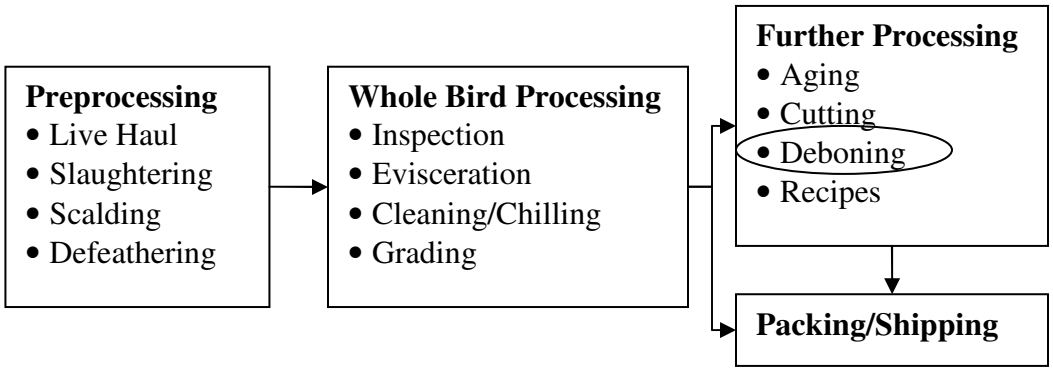


Figure 1.6: Poultry Processing

The processing operation begins with the delivery of the live product to the processing facility. Once the live poultry has been unloaded the birds are slaughtered and defeathered. Whole bird processing then prepares the carcasses for either a further processing operation or packaging and shipping of whole product. Product requiring further processing is refrigerated for approximately 24 hours. Depending on product requirements further processing can include the division of the carcass into halves, quarters, or eighths, breast and tenderloin deboning, and/or seasoning.

The application of wing manipulation presented in this thesis is applied to the breast deboning operation. Breast deboning is the removal of the wings and breast meat as a whole piece called the "butterfly". Currently the required cutting operations to perform the breast deboning are performed manually. The removal of the butterfly from the carcass has already been successfully automated.

### 1.4.2 Current Breast Deboning Process

The current deboning process beings with placing the chicken front half on a cone. The front half is separated from the bottom half by cutting through the carcass just below the rib cage. The locations of the cuts performed in creation of the front half is shown in Figure 1.7. The cone is designed such that the rib cage fits securely around the cone and is fixed by a prong which punctures the sternum and a slot on the back where the spine is located. An example of the cone conveyor line and be seen in Figure 1.8. Due to the design of the cone, the front half can be presented in a reasonably consistent location and orientation to the worker.

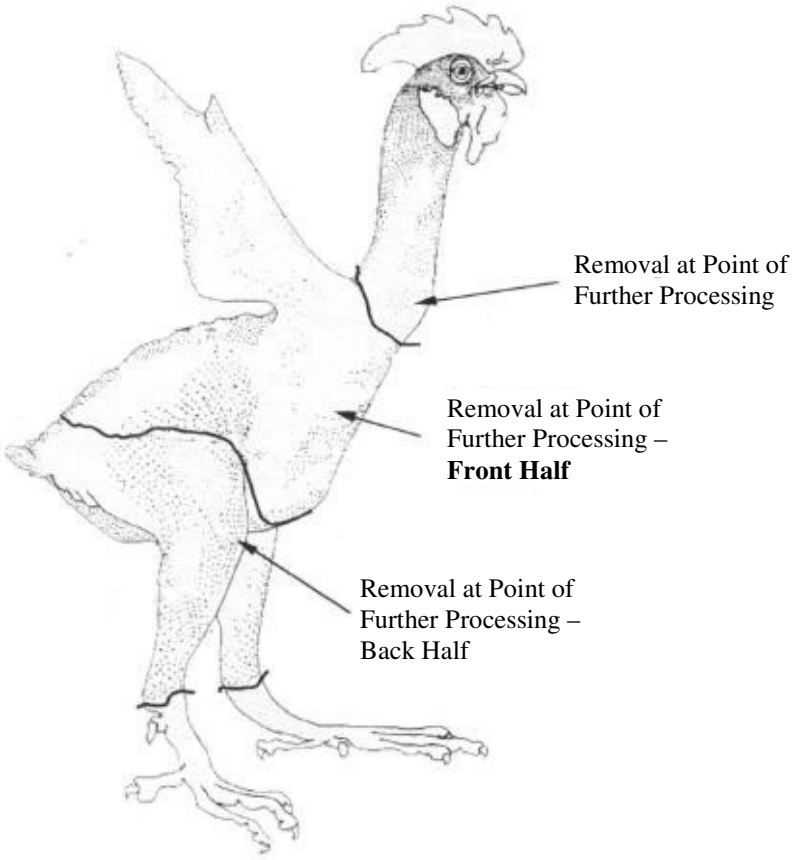


Figure 1.7: Chicken Further Processing Preparation Cuts [Robinson, 1970]

On each side of the cone conveyor there is an employee whose job it is to perform the breast deboning cuts. The cut required for removal of the butterfly performs two important tasks. The first stage of the cut severs the three major ligaments that constrain the shoulder and fix the wing to the body, as seen in Figure 1.9, and the second stage cuts down the back parallel to the scapula separating the attached breast meat. Figure 1.9(a-d) shows the location of the ligaments after the surrounding meat has been removed. As the cut progresses through each ligament the separation of the joint is clear and the locations of other internal structures are clearly visible. The chicken skeletal arrangement can be seen in Figure 1.10.

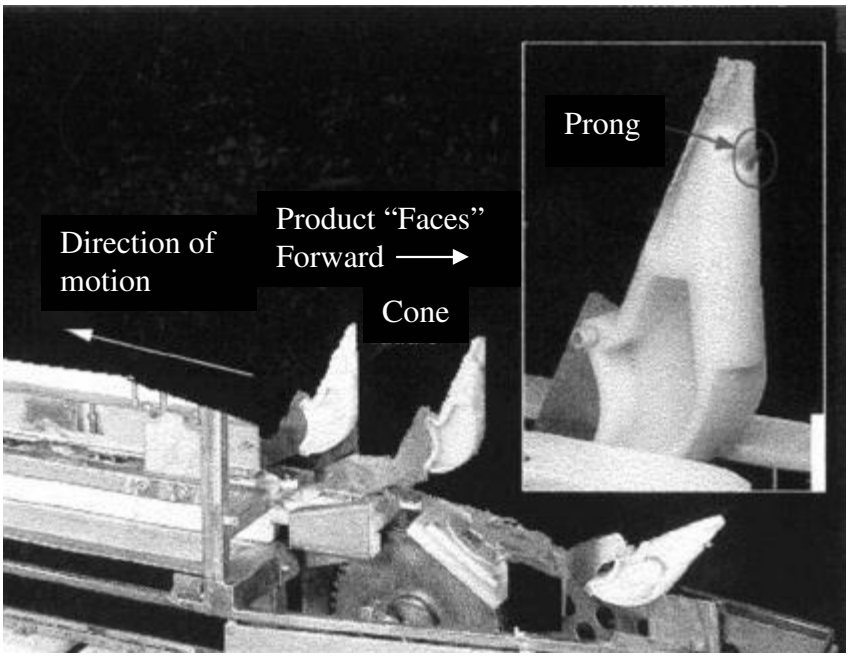


Figure 1.8: Cone Conveyor [Daley, *et al.* 1999]

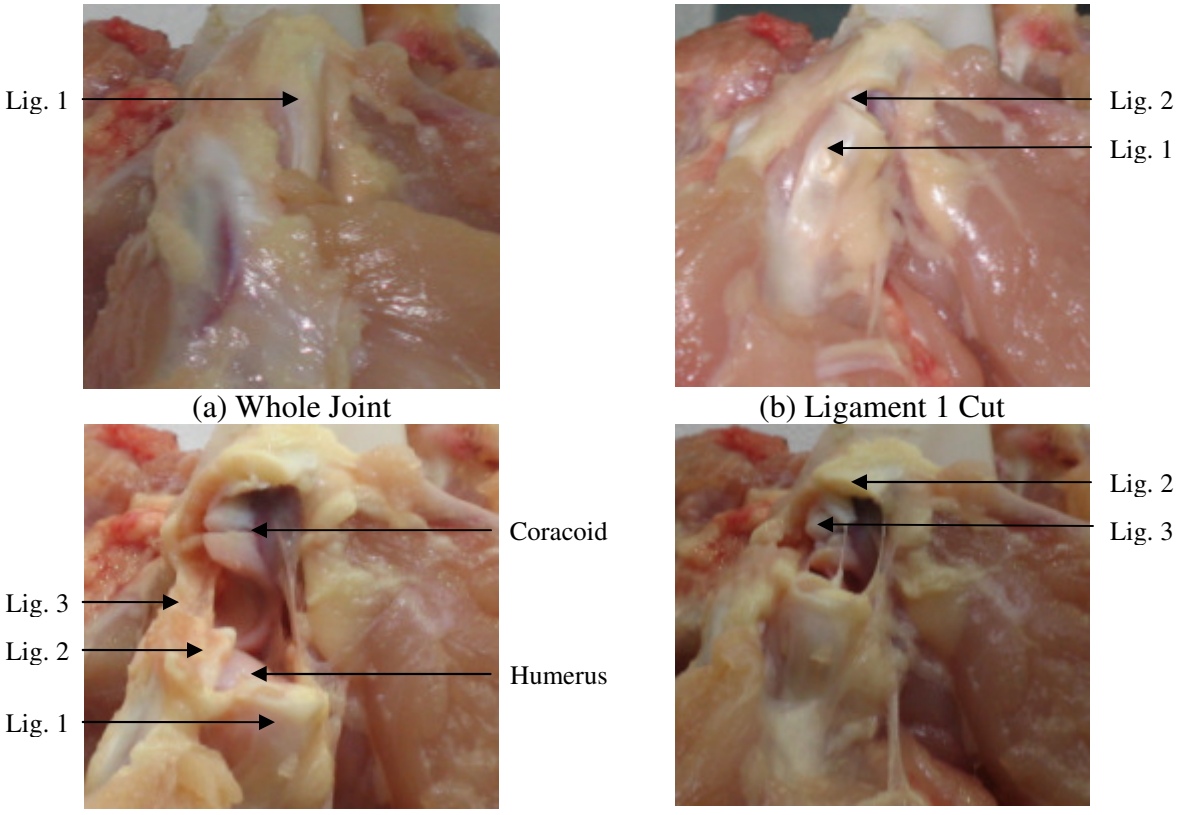


(a) Whole Joint (b) Ligament 1 Cut

(c) Ligaments 1 and 2 Cut (d) All Ligaments Cut

Figure 1.9: Ligament Cutting Sequence

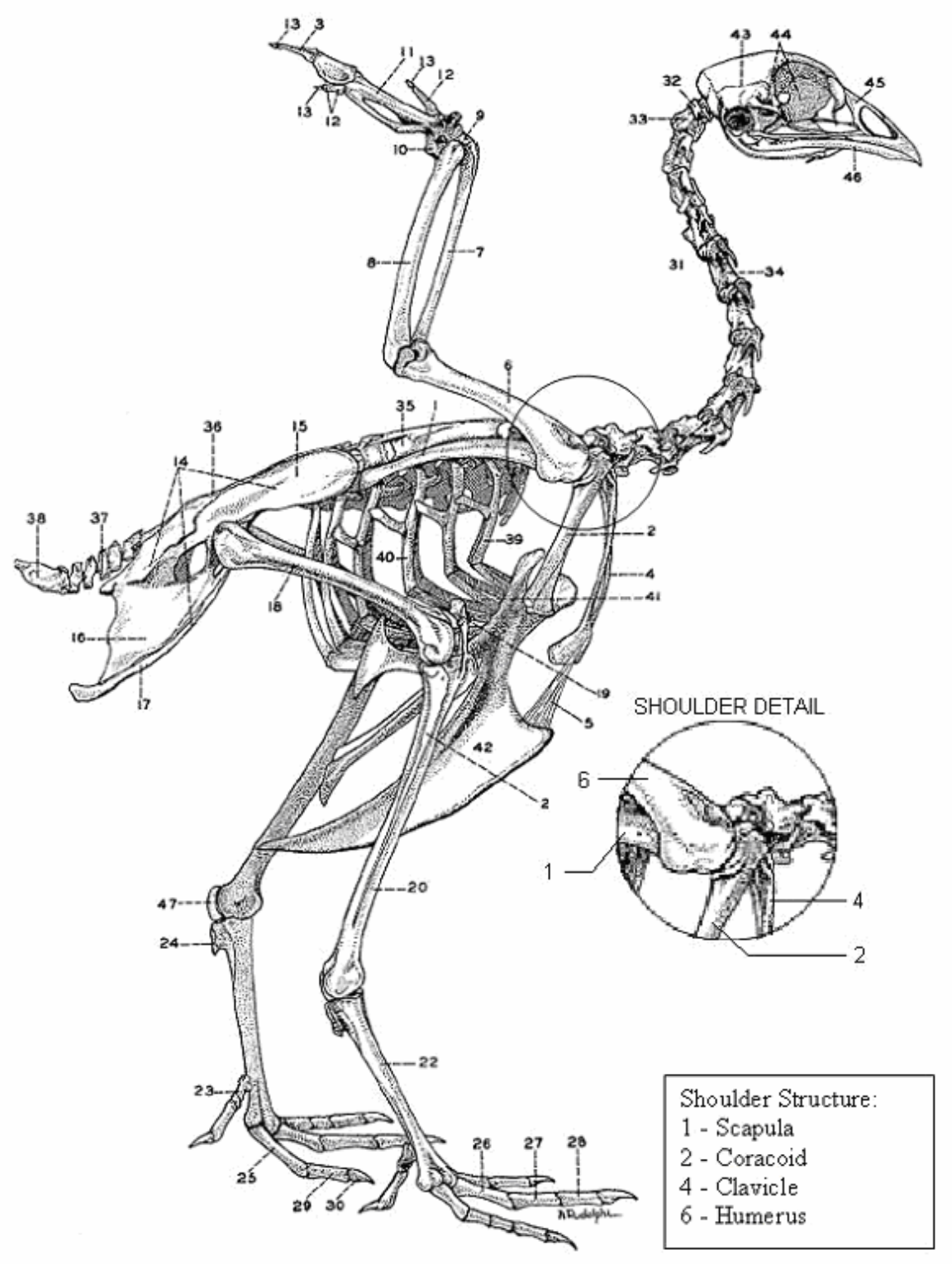


Figure 1.10: Chicken Skeleton [Chamberlain 1943]

## 1.5 Proposed Solution and Expected Contributions

The objective of the automated deboning system is to accurately perform the shoulder cut associated with the front half deboning operation. This involves knowledge of the effects of wing manipulation on the cutting path, cutting operation, as well as tasks used in locating internal structure such as needle probing. In addition the automation should improve upon previous attempts as well as improving or at least matching yield produced by the manual workers.

The proposed solution is via implementation of a wing manipulation model as well as the knowledge gained through experimentation on the effects of manipulation on needle probing and cutting tasks. The concentration of this research is on the development of a knowledge base as to how manipulation can be implemented to increase accuracy, and decrease forces, as well as presenting the internal structure with a desired pose and tension during common cutting or probing tasks.

In further research, the cutting path and manipulation trajectory will be optimized to improve product yield. An existing computer vision algorithm, developed by Daley, *et al.* [1999], will be implemented and used to locate the top of the coracoid in real time and record that information for each bird as it enters the automated cutting line. A sequence of two cutters will be designed to perform the shoulder cut and the scapula cut respectively. Application of research being done on spherical motors will provide a platform on which the circular blade can be mounted and the cutting torques indirectly monitored. Cut progress as well as variation in the cutting path through force feedback can be implemented by monitoring the torques experienced by the motors.

The research presented here has identified a problem with the current understanding of cutting and probing tasks. All of the research up to now has neglected the effects of manipulation on biological systems. The contributions of this research include a manipulation assisted automation of the poultry processing shoulder cutting operation. Also, the effects of manipulation on common needle insertion tasks is experimentally determined which provides evidence that proper manipulation improves accuracy and decreases required insertion forces. The contributions of this research extend well beyond poultry processing, several areas such as surgery, orthopedics, and acupuncture all can benefit from the application of manipulation to various biological structures.

## 1.6 Thesis Outline

The objective of this thesis is to develop an understanding of the impact of manipulation on probing and cutting operations as well as to show an application to the automation of a cutting task.

Chapter II, the development of the models used in characterizing the biological materials and manipulations are presented. This establishes the background for the development of a joint kinematic model, a quasi-static manipulation model for any skeletal joint, the forces expected during cutting of biological materials, as well as the modeling of forces associated with needle insertion tasks.

Chapter III shows the development of a ligament mechanics model as well as characterizing the effect of meat on the manipulation force. It also shows how the modeling of biological systems is very difficult due to the variations found in materials properties, skeletal dimensions, and other anatomy.

Chapter IV explores the effects of limb manipulation on needle insertion accuracy, and required forces. A series of tests are run to establish the placement errors and needle insertion forces between free and manipulated wing conditions. Needle insertion forces are also used to develop force signatures for various biological structures, and then applied to determine the underlying structure during a probing task.

In Chapter V, an application of limb manipulation to poultry processing is shown. An investigation into the proper cutting instrument is presented. The needle insertion signatures developed in Chapter 4 are then used to determine the desired cutting height for automation. A simplified cutting path is developed as well as the proper manipulation scheme. The breast deboning operation is then performed using an automated cutter with a circular blade, under proper manipulation. The automation of the breast deboning operation is shown to be feasible by implementing a manipulation system along with a simplified cutting path.

Chapter VI discusses the final conclusions and applications of the work presented in this thesis as well as some suggestions as to what future research can be done to improve and extend this thesis' applications.

# CHAPTER 2: MANIPULATION MODEL AND THEORY

This chapter develops the models for predicting the forces that will be encountered while performing a limb manipulation and cutting procedures. Limb manipulations can be found in use in several areas such as orthopedic rehabilitation, surgery, as well as poultry processing. Prediction of the forces required to perform limb manipulations will aide in determining what manipulation should be implemented for a given situation.

## 2.1 Joint Model

This section formulates the shoulder joint kinematics, beginning with defining the joint parameters affected by wing manipulation. A set of coordinate frames is then defined and the rotation matrices and translation vectors to transform between each are derived. A wing manipulation is applied and the resulting coordinate transformations are used in defining the new ligament to humerus attachment points. Finally, the positions of the ligament attachments and their respective direction unit vectors are determined.

### 2.1.1 Joint Parameters

Figure 2.1 shows the bone structure of the shoulder joint, which consists of the coracoid, humerus, scapula, and clavicle, and their position relative to the body of the bird. The humerus is manipulated at the shoulder joint relative to the fixed coarcoid, scapula, and clavicle. The shoulder joint naturally has three DOFs due to its ball and socket type construction. Due to the deformability of the connective tissues supporting

the joint it is possible to attain limited translational motion of the humerus relative to the fixed portion of the joint.

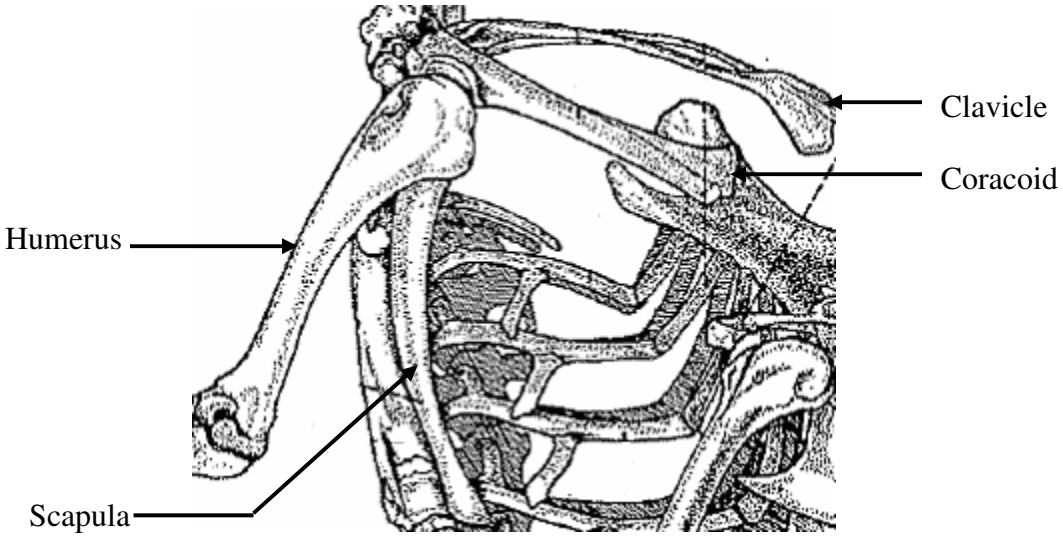


Figure 2.1: Chicken Shoulder Skeletal Anatomy [Chamberlain 1943]

Figure 2.2 shows the locations and orientations of the three coordinate frames as well as the joint parameters used in this formulation. The parameters that describe the joint kinematics include the joint element positions ($\vec{O}_c$, $\vec{O}_f$), relaxed joint element orientation ($\theta_X$, $\theta_Y$, $\theta_Z$), and connective tissue attachment locations ($\vec{L}_{1c}, \vec{L}_{2c}, \vec{L}_{3c}$, $\vec{\ell}_{1h}$, $\vec{\ell}_{2h}$, $\vec{\ell}_{3h}$). The inertial frame $X_cY_cZ_c$ is fixed at the point of rotation formed by the coracoid and humerus as denoted in Figure 2.2, where $Z_c$ points upwards and the $X_c$ axis in the direction of the bird motion. The $X_fY_fZ_f$ frame is fixed at the manipulation point of the humerus in its relaxed position. The $Z_f$ axis is along the major axis of the humerus, and the $X_f$ axis lies in the $X_cZ_c$ plane. The $x_my_mz_m$ coordinate system initially aligns with $X_fY_fZ_f$.

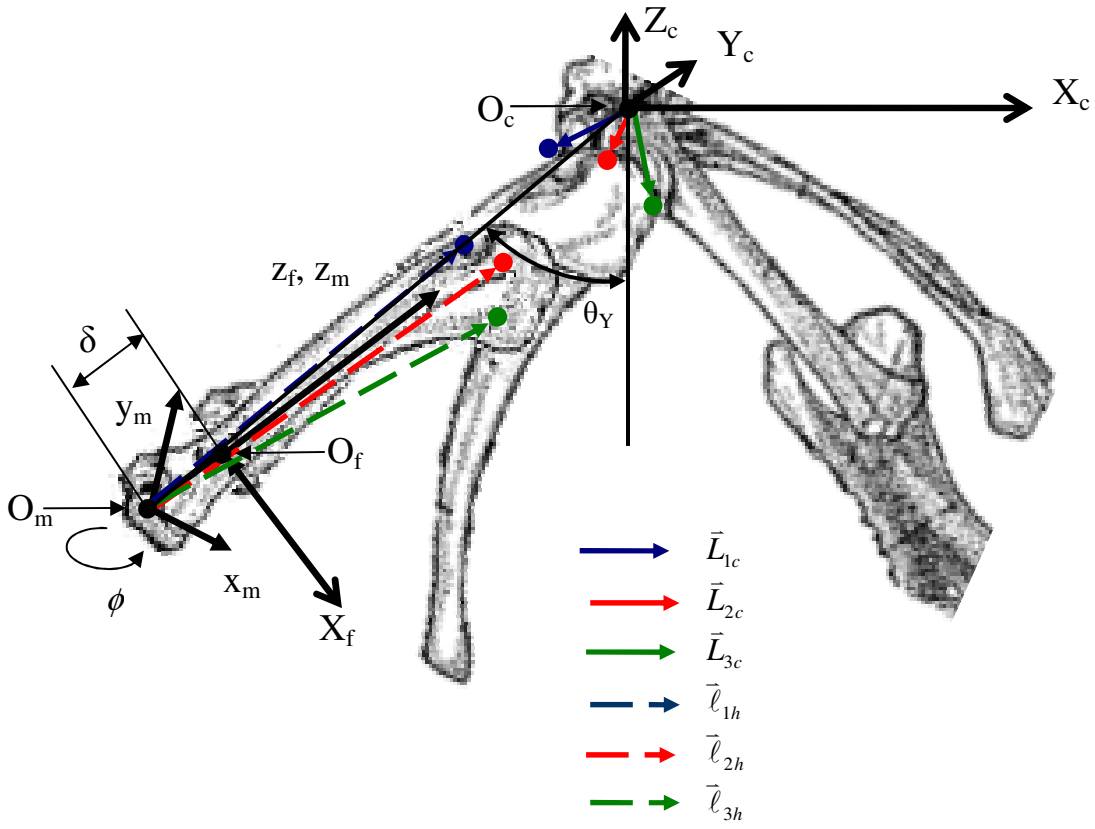


Figure 2.2: Chicken Shoulder Parameters

The vectors $\vec{L}_{1c}$, $\vec{L}_{2c}$ and $\vec{L}_{3c}$ are the ligament to coracoid attachment point locations in the fixed frame, C, and the vectors $\vec{\ell}_{1h}$, $\vec{\ell}_{2h}$ and $\vec{\ell}_{3h}$ are the ligament to humerus attachment point locations in the manipulated frame, m. The points $O_c$, $O_f$, and $O_m$ are the origins for each coordinate frame.

2.1.2 Joint Kinematics

The formulation of the joint kinematics is necessary in the determination of the ligament position and stretch given a known manipulation. The joint kinematic model determines the locations of each ligament connection point in space and thus calculates the individual ligament stretches and directions.

The basis of a kinematic model is coordinate transformations through rotation and translation. The rotation matrices from one coordinate frame to another are defined by

$$\theta_X = -\tan^{-1}\left(\frac{O_{fY}}{O_{fZ}}\right) \tag{2.1}$$

$$\theta_Y = -\tan^{-1}\left(\frac{O_{fX}}{\sqrt{O_{fX}^2 + O_{fY}^2 + O_{fZ}^2}}\right) \tag{2.2}$$

$$[R_{mc}] = \begin{bmatrix} \cos\theta_z \cos\theta_y & \sin\theta_z \cos\theta_x + \cos\theta_z \sin\theta_y \sin\theta_x & \sin\theta_z \sin\theta_x - \cos\theta_z \sin\theta_y \cos\theta_x \\ -\sin\theta_z \cos\theta_y & \cos\theta_z \cos\theta_x - \sin\theta_z \sin\theta_y \sin\theta_x & \cos\theta_z \sin\theta_x + \sin\theta_z \sin\theta_y \cos\theta_x \\ \sin\theta_y & -\cos\theta_y \sin\theta_x & \cos\theta_y \cos\theta_x \end{bmatrix} \tag{2.3}$$

$$[R_{mf}] = \begin{bmatrix} \cos\phi & \sin\phi & 0 \\ -\sin\phi & \cos\phi & 0 \\ 0 & 0 & 1 \end{bmatrix} \tag{2.4}$$

For Equation (2.4) $\phi$ is the wing twist manipulation.

Upon application of a pull $\delta$ and twist $\phi$ manipulations to the wing the attachment points of the ligaments to the humerus move in relation to the stationary coracoid frame, defined by the following transformations:

For the remainder of this derivation, the index *j* is used to represent each of the ligaments in the joint.

$$\left[\hat{R}_{mf}\right]=\begin{bmatrix}\left[R_{mf}\right] & \begin{bmatrix}0\\0\\-\delta\end{bmatrix}\\ 0 & 1\end{bmatrix} \tag{2.5}$$

$$\left[\hat{R}_{cm}\right]=\begin{bmatrix}\left[R_{cm}\right] & \vec{O}_f\\ 0 & 1\end{bmatrix} \tag{2.6}$$

$$\begin{bmatrix}\vec{L}_{jh}\\1\end{bmatrix}=\left[\hat{R}_{cm}\right]\left[\hat{R}_{mf}\right]\begin{bmatrix}\vec{l}_{jh}\\1\end{bmatrix} \tag{2.7}$$

The ligament stretch is determined by calculating the change in ligament length from its length at the relaxed wing position to its length after the applied manipulation. The non-manipulated ligament to humerus attachment points, $\vec{L}_{jh}^{free}$, are calculated in the same way as $\vec{L}_{jh}$ but with no manipulation, therefore $\delta=\phi=0$.

The individual ligament stretches, $\Delta_j$, are calculated by

$$\Delta_j=\left|\vec{L}_{jc}-\vec{L}_{jh}\right|-\left|\vec{L}_{jc}-\vec{L}_{jh}^{free}\right| \tag{2.8}$$

For application in force definition the ligament direction unit vectors, $\vec{u}_j$, and attachment point vectors, $\vec{\rho}_j$, are defined by the following:

$$\vec{u}_j=\frac{\vec{L}_{jc}-\vec{L}_{jh}}{\left|\vec{L}_{jc}-\vec{L}_{jh}\right|} \tag{2.9}$$

$$\vec{\rho}_j=\vec{L}_{jh}-\vec{O}_m \tag{2.10}$$

The final output of the kinematic model is a graphical representation of the location of the ligament attachments and the humerus after each step in a specified manipulation.

## 2.2 Quasi-Static Manipulation Force Model

The quasi-static force model is used to determine the forces and moments that are be present at the point of wing manipulation over a specified manipulation. This section formulates the quasi-static model.

A ligament mechanics model, represented in Equation (2.11) as a function of $\overline{\Delta}_j$, allows for the calculation of individual ligament tension by

$$\vec{T}_j = f\left(\Delta_j\right)\vec{u}_j \tag{2.11}$$

A change of coordinate frame is necessary to represent the manipulation force and moment in the manipulated frame (m-frame).

$$\vec{f}_m = \left[R_{m,c}\right]\sum_{j=1}^{n}\vec{T}_j \tag{2.12}$$

$$\vec{m}_m = \left[R_{m,c}\right]\sum_{j=1}^{n}\vec{\rho}_j \times \vec{T}_j \tag{2.13}$$

The above equations govern the quasi-static model developed to predict the limb manipulation forces under a specified manipulation trajectory. In order to successfully implement this model the joint parameters and the ligament mechanics model must be developed. Chapter 3 discusses the development of the required model and parameters for a specific application, a chicken wing manipulation.

## 2.3 Model Summary

This section summarizes the flow of data through the joint kinematic model and the quasi static manipulation force model. Figure 2.3 shows the flow chart of the joint kinematic algorithm consisting of the following processes: development of coordinate transformations, transformation of ligament attachment points, and calculation of manipulated ligament stretch, direction, and location.

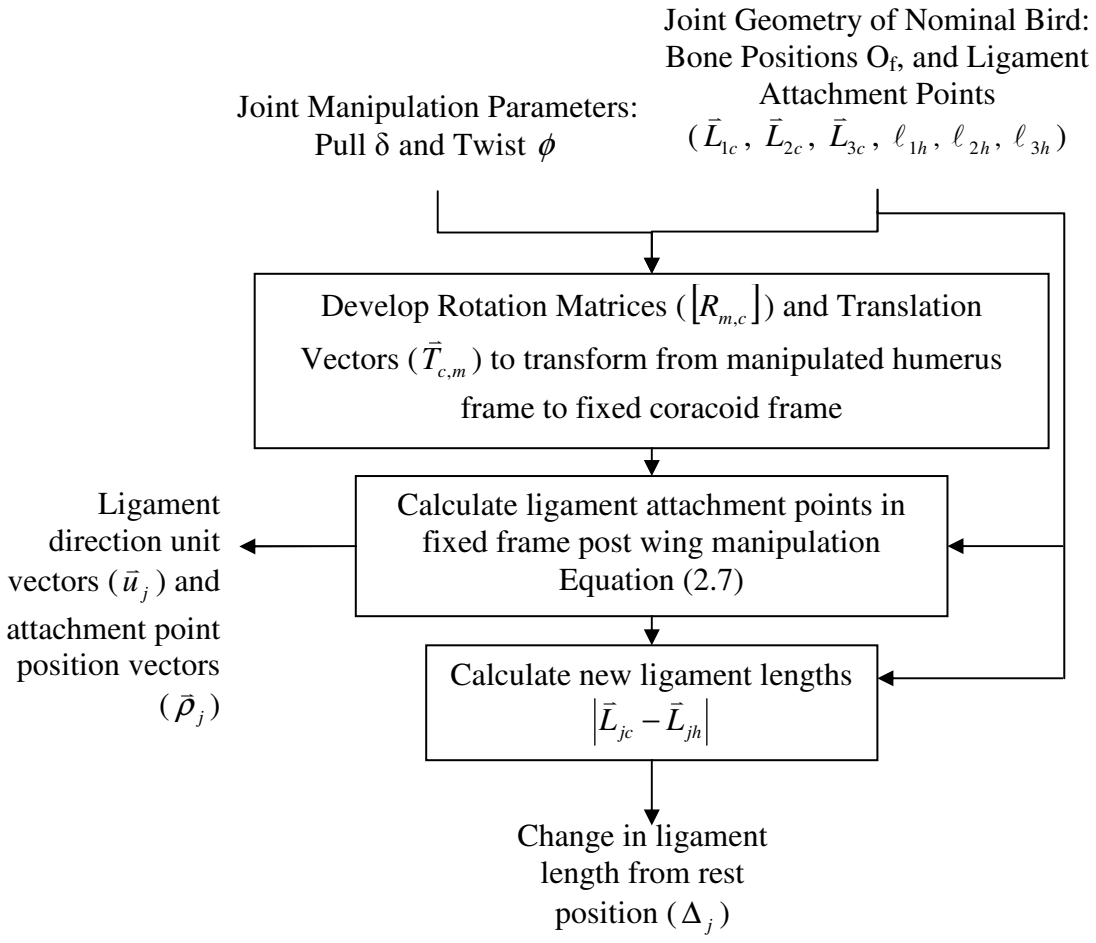


Figure 2.3: Joint Kinematic Model Algorithm Schematic

Figure 2.4 is the flow chart for the quasi-static model, consisting of

1. Input of ligament stretch from the joint kinematic model,
2. Application of the ligament mechanics model,
3. Calculation of ligament tensions and,
4. Calculation of the experienced manipulation forces and moments.

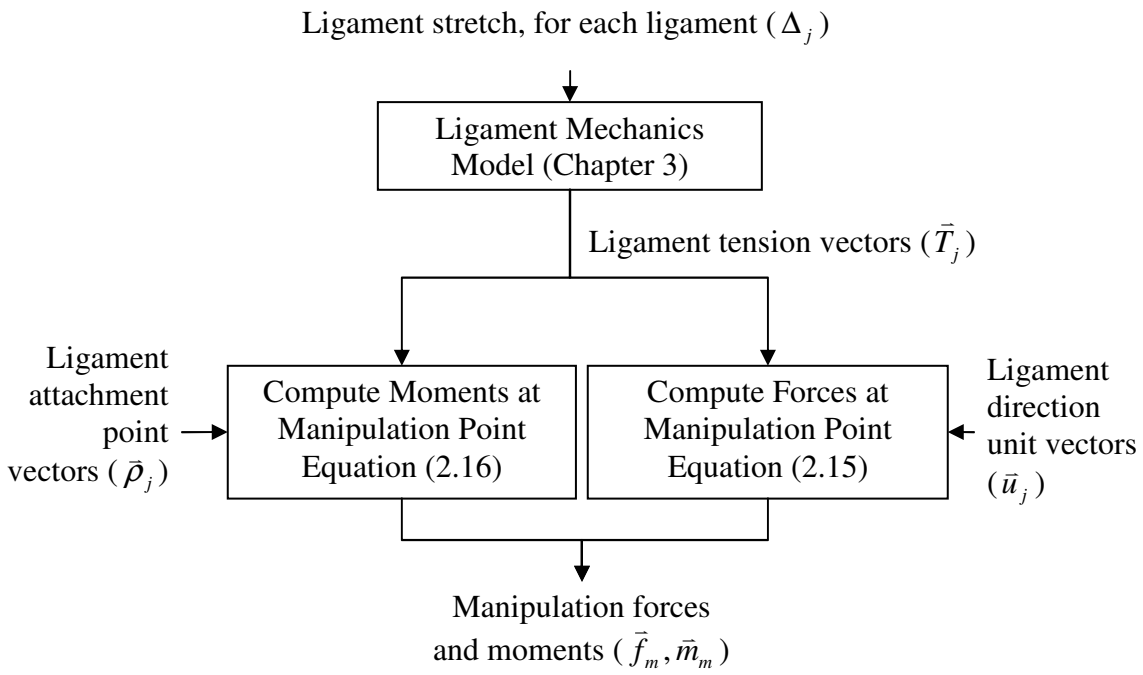


Figure 2.4: Quasi-Static Model Schematic

## 2.4 Principles of Cutting

This section presents an approach based on the work/energy method, suggested by Atkins and Jeronimidis [2004], on modeling shear and compressive cutting forces experienced during the cutting of biomaterials.

As illustrated in Figure 2.5, the cutter moves vertically and horizontally. This motion results in compression due to the vertical displacement and the shearing due to horizontal displacement. The work done during cutting is based around the following equation:

$$Kdk = Rwda + d(\text{friction}) \tag{2.14}$$

where $dk$ is an incremental displacement in the direction of the cutting force $K$; $a$ is the cut depth; $w$ is the width (or thickness) of the material being cut; and $R$ is the fracture toughness of the material measured in N/m. Material fracture toughness is a measure of the resistance of a material to failure due to fracture. Engineering material fracture toughness values are generally available, but it is recommended to determine material and condition specific fracture toughness through experimentation. The work has been based on the following assumptions:

1. Cutting produces floppy undistorted offcuts. This results in no energy being spent to permanently deform the offcuts.
2. The cutter experiences no friction during the cut. Therefore, there is no energy loss due to friction between the material and blade.

In the case of compression cutting, assuming that the crack does not propagate faster than the blade advances ($da = dk$) and the friction on the blade is small, Equation (2.14) can be simplified to

$$K = Rw \tag{2.15}$$

Figure 2.5 shows a schematic of a blade cutting a deformable material.

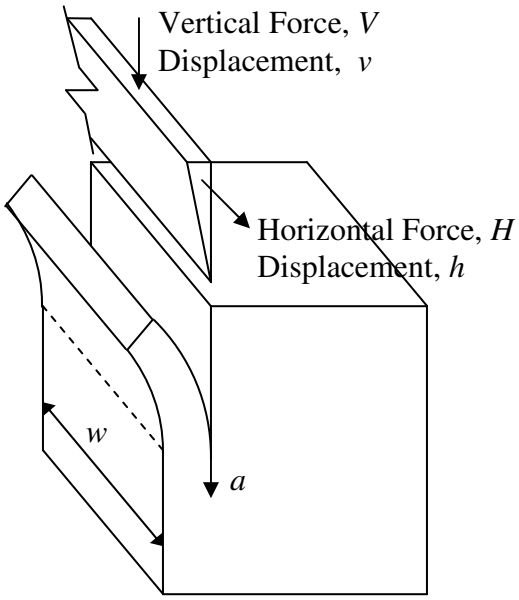


Figure 2.5: Cutting by Pressing and Slicing

During cutting by pressing and slicing assume that in unit time $V$ moves through $dv$ and $H$ through $dh$ and that the width of the blade is greater than the width of material, thus maintaining a constant cut length. The incremental work done in slice/push cutting can be expressed as

$$Vdv + Hdh = Rwdv \tag{2.16}$$

giving

$$(Rw - V)dv = Hdh \tag{2.17}$$

or by considering the resultant force and displacement

$$\sqrt{(V^2 + H^2)\left[(dv)^2 + (dh)^2\right]} = Rwdv \tag{2.18}$$

where the resultant force and displacement are given by $\sqrt{V^2 + H^2}$ and $\sqrt{dv^2 + dh^2}$ respectively.

The ratio of the horizontal to vertical incremental displacement is given by $\xi = dh / dv$ thus Equations (2.17) and (2.18) become

$$(Rw - V) = H\xi \tag{2.19}$$

and

$$\sqrt{(V^2 + H^2)(1 + \xi^2)} = Rw \tag{2.20}$$

Replace $V$ by $Rw - H\xi$ and manipulate to develop the normalized horizontal (slice) and vertical (compressive) cutting forces.

$$\frac{H}{Rw} = \frac{\xi}{1 + \xi^2} \qquad \text{and} \qquad \frac{V}{Rw} = \frac{1}{1 + \xi^2} \qquad (2.21\ \text{a,b})$$

Plotting of the variation of the normalized cutting forces with the slice/push ratio shown in Figure 2.6 clearly shows the significant reduction of both the shear and compressive cutting forces as the slice/push ratio increases. Along with the theoretical cutting forces, experimental data from cutting cubes of potato is plotted in Figure 2.6.

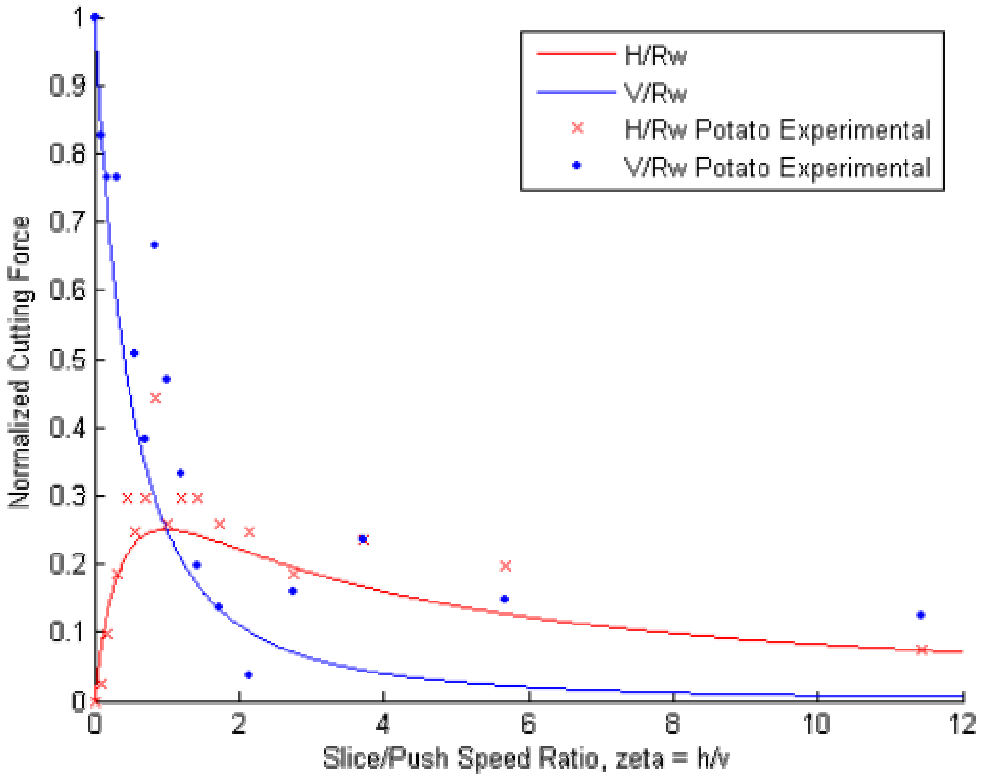


Figure 2.6: Variation of Normalized Cutting Forces with 'Slice/Push' Speed Ratio

Preliminary experimentation on the cutting of meat shows that compressive cutting of meat requires very high forces due to the significant deformation of the meat upon contact with the blade. The application of shearing motion allows for decrease in required compression and resulted in a characteristic similar to that shown in Figure 2.6.

## 2.5 Membrane Puncture

This section presents the development of membrane puncture force models. Puncturing of membranes occurs in any cutting or needle probing task performed on biomaterials. Several studies have been performed to characterize the needle insertion forces. Okamura, *et al.* [2004] presents an experimental investigation into the force modeling of the interaction between needles and biological materials. They developed an

analytic solution to modeling the insertion forces. They characterized the liver stiffness and puncture force by fitting a second order polynomial to the force vs. displacement results as well as producing an experimentally determined force threshold at which initial puncture occurs. The coefficients $a_1$ and $a_2$, of the polynomial, Equation (2.22), are material dependant and therefore experimentation need be performed on any material of interest.

$$f(z) = a_1 z + a_2 z^2 \tag{2.22}$$

There has been no theoretical basis developed to model needle insertion and membrane puncture forces. Currently, all needle insertion simulations are dependant on experimentally developed analytic models.

## 2.6 Concluding Remarks

This chapter presents a theoretical basis for the experimentation to be performed in the following chapters. Section 2.1 introduces the joint layout, defining parameters, and kinematic model. Section 2.2 develops upon the kinematic model by applying a ligament force vs. displacement model to predict manipulation forces given a limb manipulation. Section 2.4 discusses the work/energy method of modeling cutting forces in compression and shear directions. The theoretical forces are shown in comparison to preliminary experimental data on the cutting of a firm yet deformable biomaterial. Section 2.5 concludes the theoretical overview with an introduction to the methods used in modeling needle insertion and puncture. Thus far there is no solid theoretical backing to needle insertion and puncture. All modeling of these actions is through the use of analytic model development.

# CHAPTER 3: EXPERIMENTAL DETERMINATION OF CHICKEN SHOULDER MODEL PARAMETERS

This chapter begins with developing an empirical model to characterize the mechanics of the chicken shoulder ligaments. Next, the characterization of the meat influence on manipulation force is determined by comparison of the experimental manipulation results to the theoretical manipulation force.

The values for ligament cross-sectional area, attachment point locations, and humerus rest position are determined by measurement and averaging using several nominal sized birds. All experiments are performed on nominal sized birds to minimize the effects of specimen variation.

## 3.1 Ligament Mechanics Model

In order to develop a model that will accurately describe the forces encountered during joint manipulation it is necessary to characterize the mechanics of the main elements in the system. In the case of a chicken shoulder, three of the major ligaments that support the joint must be cut. The following section contains the experimental setup, results, and development of a ligament mechanics model.

### 3.1.1 Experimental Setup

In order to determine the ligament characteristics they needed to be tested in an environment that is similar to the state that they will be in during the cutting operation. The coracohumeralis ligament was chosen as the test sample due to its size, location, and ease of singulation. The other major ligaments are in locations difficult to remove

without damaging the ligament itself. In an effort to not alter the ligament characteristics, the ligament was not separated from either the humerus or the coracoid. By retaining the bone connection on both sides of the ligament, it is possible to apply a tension load to the sample without the problems that arise due to clamping of free ends of the ligament. To minimize variation in measurement the cross sectional area of the ligament was determined by first twisting the ligament slightly in order to develop an elliptical shaped cross section. The major and minor diameters of the resulting ellipse were then measured with calipers are recorded. Figure 3.1 shows the experimental apparatus. The shoulder screws provide a surface for the humerus to pull against while the coracoid, attached to a 6 axis force/torque sensor and a six degree of freedom robot arm, is pulled at a constant velocity. The pulling action performed by the robot causes stretching of the ligament.

In developing the ligament mechanics model, the following assumptions were made. These assumptions were made to facilitate the modeling of the complex structure in such a way that it will be accurate within the application conditions.

1) The ligament acts as a non-linear spring.
2) There are no dynamic effects because of low stretch rate as well as difficulty in experimentally determining damping or inertial parameters for ligaments.

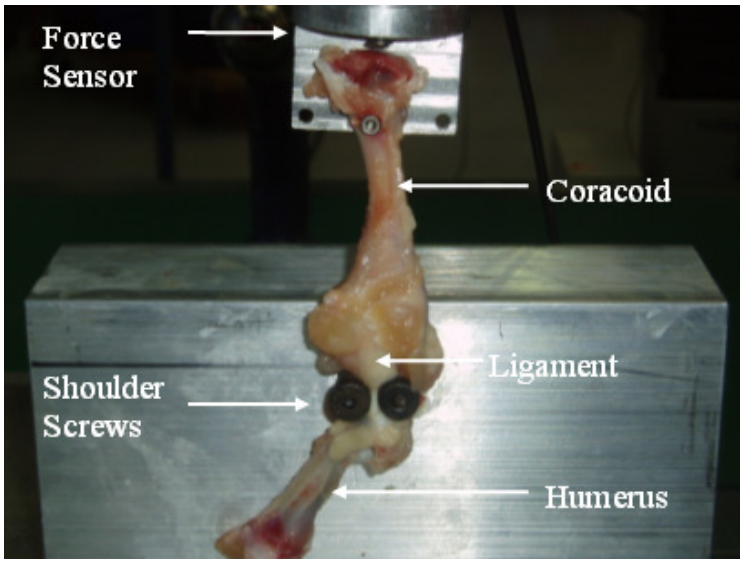

Figure 3.1: Ligament Testing Apparatus

### 3.1.2 Experimental Results

Recording the robot velocity as well as the tensile force at the force sensor over time, it is possible to produce the force vs. stretch plots for each sample. The force characteristics for the eight ligament samples are shown in Figure 3.2.

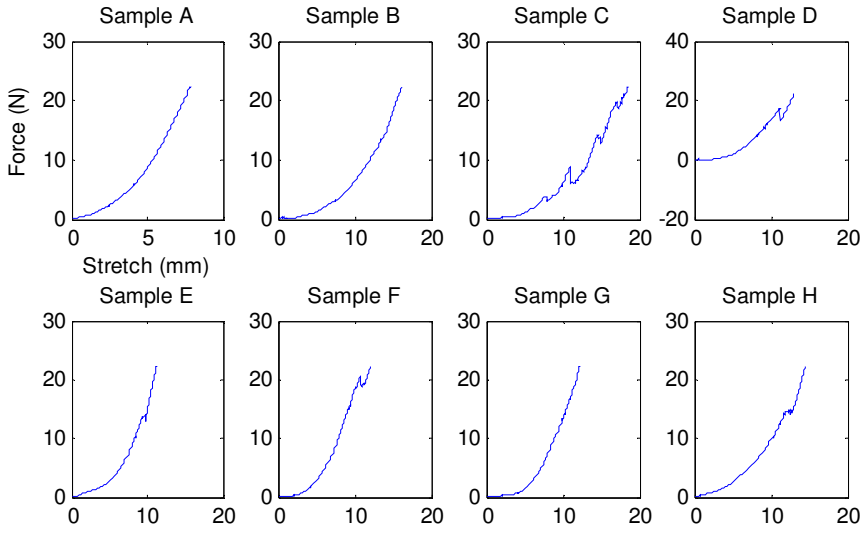

Figure 3.2: Individual Ligament Force vs. Stretch Characteristics

The forces for each sample were then normalized by the ligaments cross sectional area. The results are shown in Figure 3.3.

3.1.3 Non-Linear Spring Model

By modeling the ligaments as non-linear springs, it is possible to derive a constitutive equation that can characterize the force-displacement relationship of the test samples. The experimental data of each sample in Figure 3.3 suggests the non-linear characteristic form

$$\frac{F_o}{A} = C_o x^{m_o} \tag{3.1}$$

Where $F_o$ is the tensile force acting on the ligament; A is the ligament cross sectional area; $C_o$ is and $m_o$ are material specific constants; and $x$ is the stretch of the ligament. Equation (3.1) can be rewritten as

$$\log F_o = \log C_o + m_o \log x$$

As expected the experimental data is linear on a log-log plot shown in Figure 3.4. The parameters, $C_o$ and $m_o$, for the specific ligament are respectfully the intercept and slope of a straight line fit to the experimental data in Figure 3.4. The individual values are show in Table 3.1.

Table 3.1: Individual Ligament Parameter Values

| **Sample** | **C** | **m** |
|---|---|---|
| A | $33\times10^{-4}$ | 2.2 |
| B | $4.5\times10^{-4}$ | 2.2 |
| C | $5.0\times10^{-4}$ | 2.4 |
| D | $1.8\times10^{-4}$ | 3.0 |
| E | $17.\times10^{-4}$ | 1.9 |
| F | $3.9\times10^{-4}$ | 2.9 |
| G | $2.9\times10^{-4}$ | 2.8 |
| H | $2.0\times10^{-4}$ | 1.8 |
| **Average** | $\mathbf{C_o = 6.7\times10^{-4}}$ | $\mathbf{m_o = 2.4}$ |

In order to further validate the power function model, it is desired for the experimental data to have a similar shape to the model and only differ by a scaling factor. This analysis is performed by dividing the experimental data by the model data. This results in an expression of the form

$$\frac{F}{F_o} = \frac{C}{C_o} x^{(m_o - m)} \tag{3.2}$$

with the resulting data plotted in Figure 3.5.

Samples B through H result in nearly constant values. The presence of these constant lines implies

$$m \approx m_o \tag{3.3}$$

and therefore

$$\frac{F}{F_o} \approx \frac{C}{C_o} \approx const. \tag{3.4}$$

Figure 3.6 is a plot of $F_o / A$ superimposed over the experimental data. The dashed lines on each side of $F_o / A$ depict an envelope created by a scaling of the coefficient, C, by ±30%.

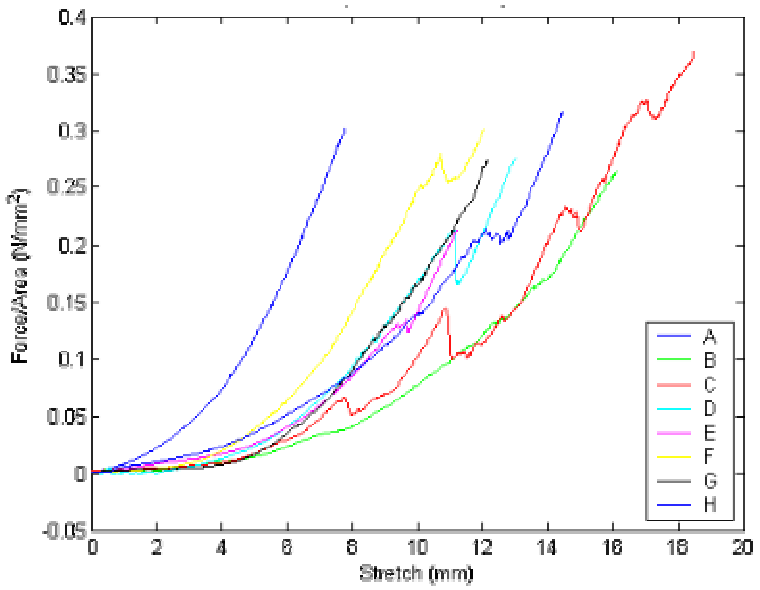


Figure 3.3: Ligament Samples Normalized by Cross-Sectional Area

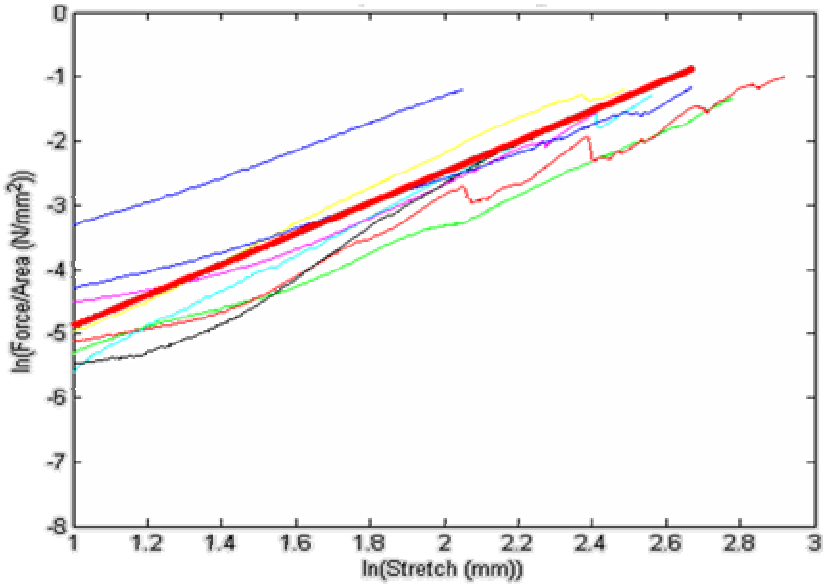


Figure 3.4: Ligament Samples Log/Log Plot

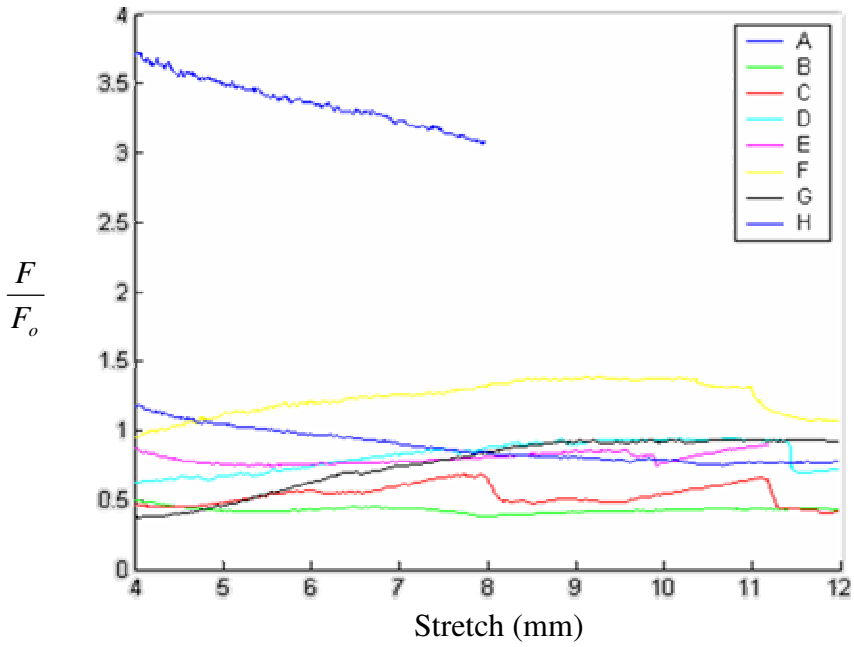


Figure 3.5: Scaling of Experimental Samples by Model

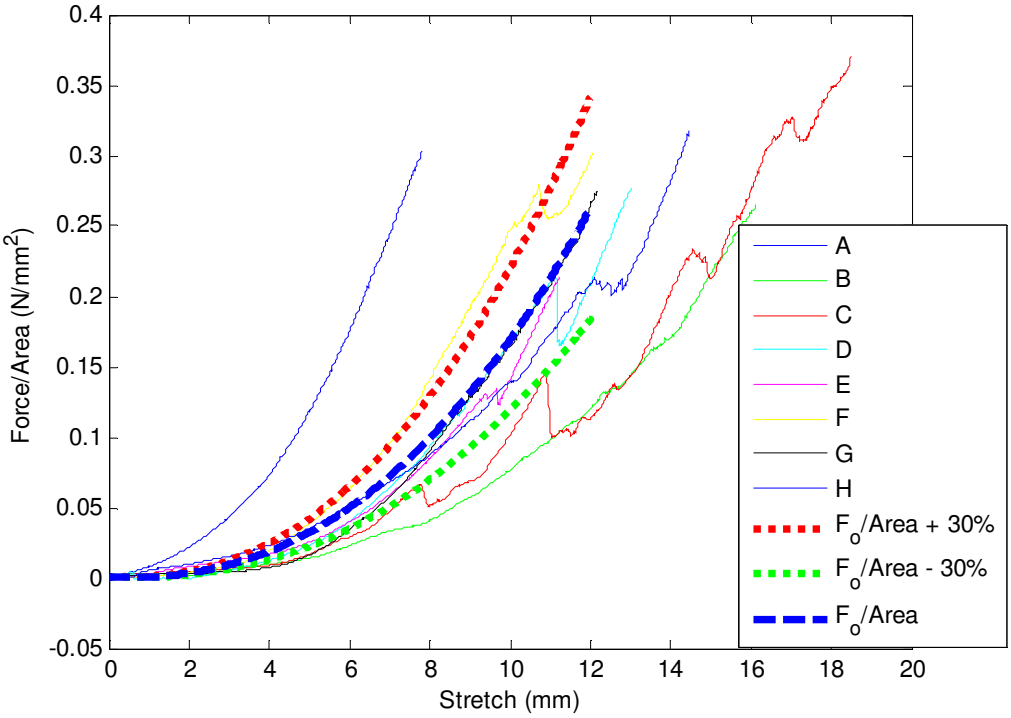


Figure 3.6: Ligament Model with ±30% Bounds

## 3.2 Meat Characterization

In order to characterize the effect due to the mechanical properties of the meat on the manipulation force the theoretical manipulation force due to ligaments must be subtracted from the experimental manipulation force. The parameter values in Table 3.2 were determined by measurement of several birds and represents the nominal bird values. The ligament cross sectional areas, $A_{c1}$ thru $A_{c3}$, were developed by approximating each ligament as having a rectangular cross section and measuring each ligament in-vivo with a set of calipers.

Table 3.2: Simulation Parameter Values

| **Humerus Rest Position (mm)** | **Value** |
|---|---|
| $\vec{O}_f = (O_{fX}, O_{fY}, O_{fZ})$ | (0, 25, 70) |
| **Ligament Attachment Points (mm)** | |
| $\vec{L}_{1c}$ | (-3, 1.6, -15) |
| $\vec{L}_{2c}$ | (1.3, 2.8, 1.5) |
| $\vec{L}_{3c}$ | (3.3, -3.0, -9.2) |
| $\vec{l}_{1h}$ | (-11.9, 3.4, 52) |
| $\vec{l}_{2h}$ | (0, -9.2, 52.5) |
| $\vec{l}_{3h}$ | (6.1, -0.9, 50.9) |
| **Cross Sectional Area ($mm^2$)** | |
| $A_{c1}$ | 15.08 |
| $A_{c2}$ | 18.06 |
| $A_{c3}$ | 9.87 |

These nominal bird parameters are used in conjunction with the input manipulation to predict the manipulation force due to ligament constraints.

### 3.2.1 Experimental Setup

In order to determine the meat characteristics, the manipulation forces imposed by the entire joint as well as strictly by the ligaments must be determined. To establish the manipulation force exhibited during a 10mm pull manipulation a force sensor was installed in series with the ABB robot. The ABB robot is used to input a 10mm step pull manipulation to the wing, at the same time the force sensor is used to record the required manipulation forces. A rigid connection was established between the force sensor and the wing in order to eliminate any spring effect due to the use of compliant materials.

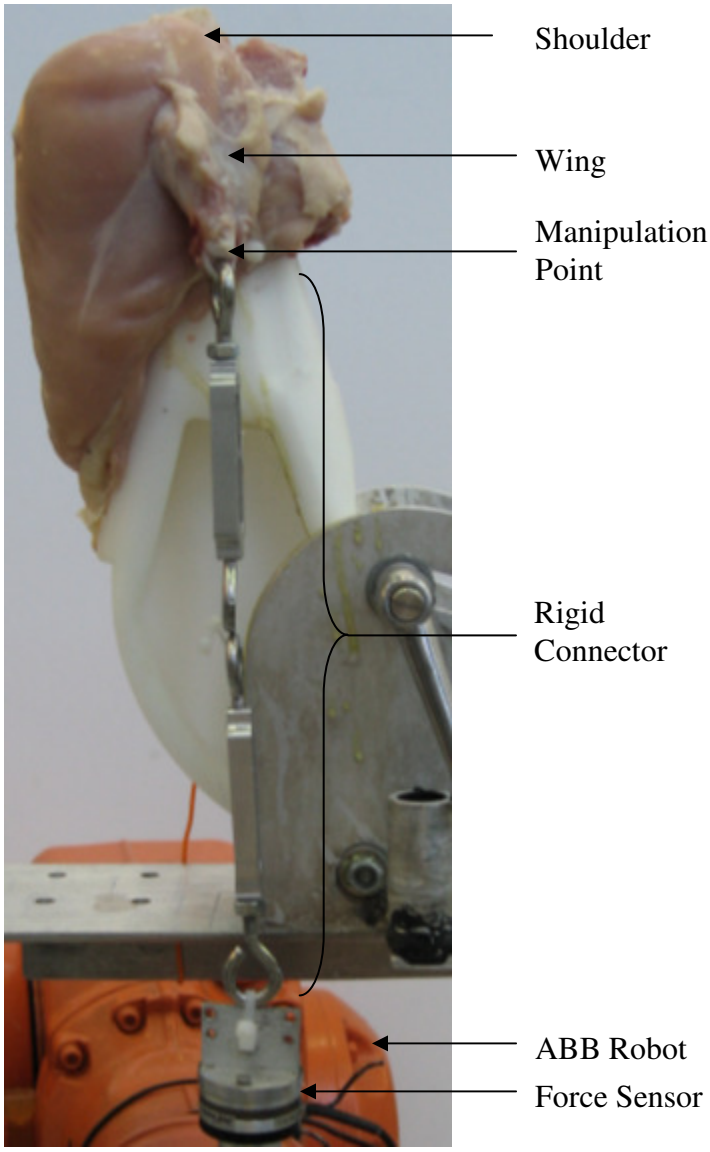


Figure 3.7: Pull Step Experimental Setup

The manipulation force due to the ligaments was then determined by removal of all tissue surrounding the joint except for the ligaments. The same manipulation was performed and the required force recorded. This manipulation force can also be determined by application of the joint model developed in Chapter 2. In the joint mechanics model it is assumed that the ligament to coracoid connection points are fixed in space due to the assumption that the coracoid and remainder of the body is rigidly

fixed. As expected this assumption does not hold in the case of large shoulder manipulations. In order to correctly predict the manipulation forces the effective ligament stretch must first be determined by measurement of the coracoid displacement under a specified manipulation.

### 3.2.2 Body Displacement Correction

Figure 3.8 shows the experimental setup used in determining the coracoid deflection. In order to correct for the coracoid displacement error the displacement is measured during a 10mm pull manipulation and then the effective pull imposed on the ligaments is calculated from the recorded image as shown in Figure 3.8(b) and (c).

(a) Coracoid Displacement Experimental Setup

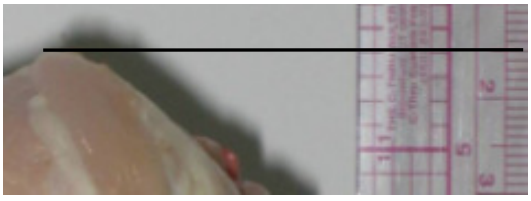

(b) Location Before Manipulation
Coracoid Height = 14.8mm

(c) Location After Manipulation
Coracoid Height = 18.5mm

Figure 3.8: Coracoid Displacement Under 10mm Pull Manipulation

Measurement of the change of position results in an effective pull manipulation of approximately 6.3mm imposed on the ligaments.

The experimental results from a 10mm pull manipulation performed on a shoulder with all the meat removed are shown in Figure 3.9.

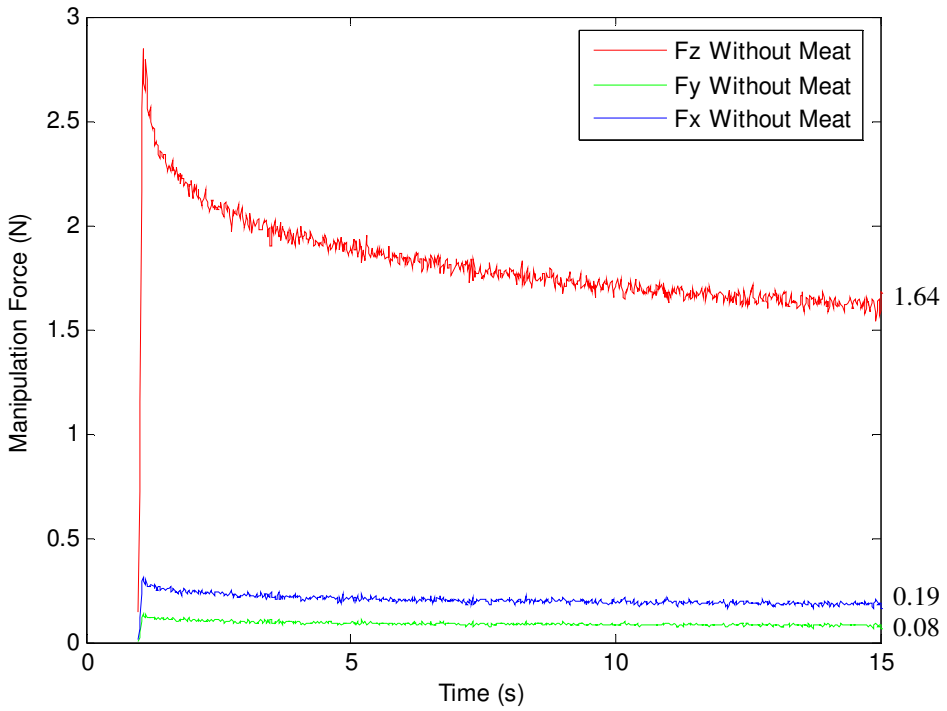


Figure 3.9: Experimental Manipulation Forces with Meat Removed, 10mm Pull

Correcting for the displacement of the coracoid and thus application of the 6.3mm pull manipulation as the manipulation input to the theoretical model results in predicted manipulation steady state forces of 1.68 N, 0.40 N, and 0.19 N for $F_z$, $F_y$, and $F_x$ respectively, as shown in Figure 3.10.

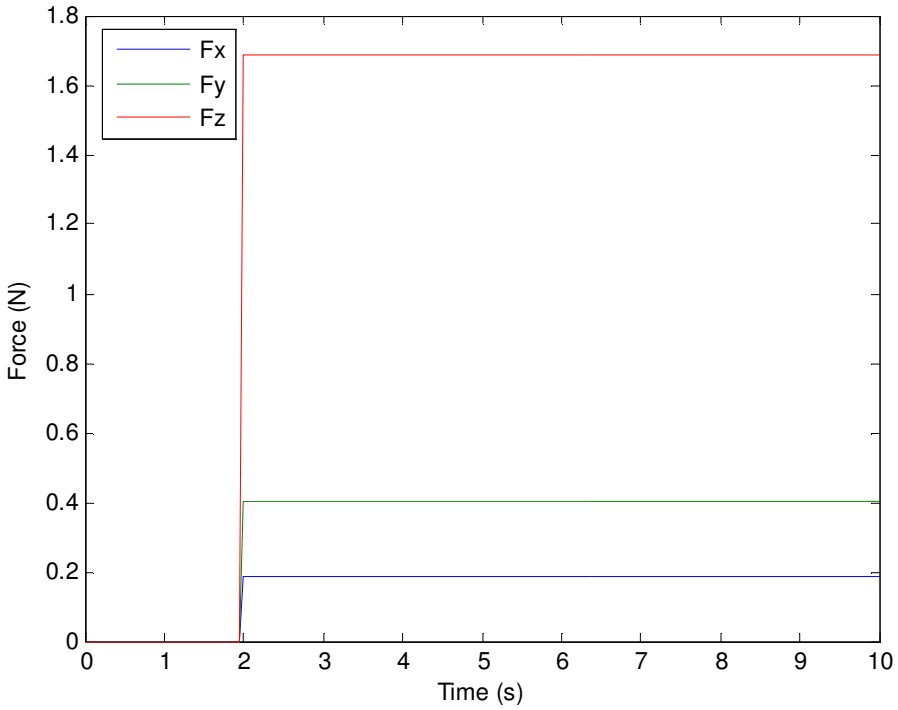


Figure 3.10: Theoretical Manipulation Forces, 6.3mm Pull

Table 3.3 compiles the data shown in Figure 3.9 and Figure 3.10 for ease of comparison.

Table 3.3: Theoretical vs. Experimental Steady State Force Comparison

| **Force** | **Theoretical (N)** | **Experimental (N)** |
|---|---|---|
| $F_x$ | 0.19 | 0.08 |
| $F_y$ | 0.40 | 0.19 |
| $F_z$ | 1.68 | 1.64 |

These force values match the experimental values closely, though there exists error in the $F_x$ and $F_y$ forces. This error is most likely due to the natural variation in internal geometry and size between the bird used during experimentation, and the nominal bird used in development of the model. The actual location of the ligament

connection points, ligament cross sectional areas, and resting wing position may vary, thus resulting in differences between experimental and theoretical manipulation forces.

Figure 3.11 shows a sample comparison between the model predicted $F_z$ manipulation force and steady state experimental results. The red line is the theoretical force and the blue dots are the steady state experimental results.

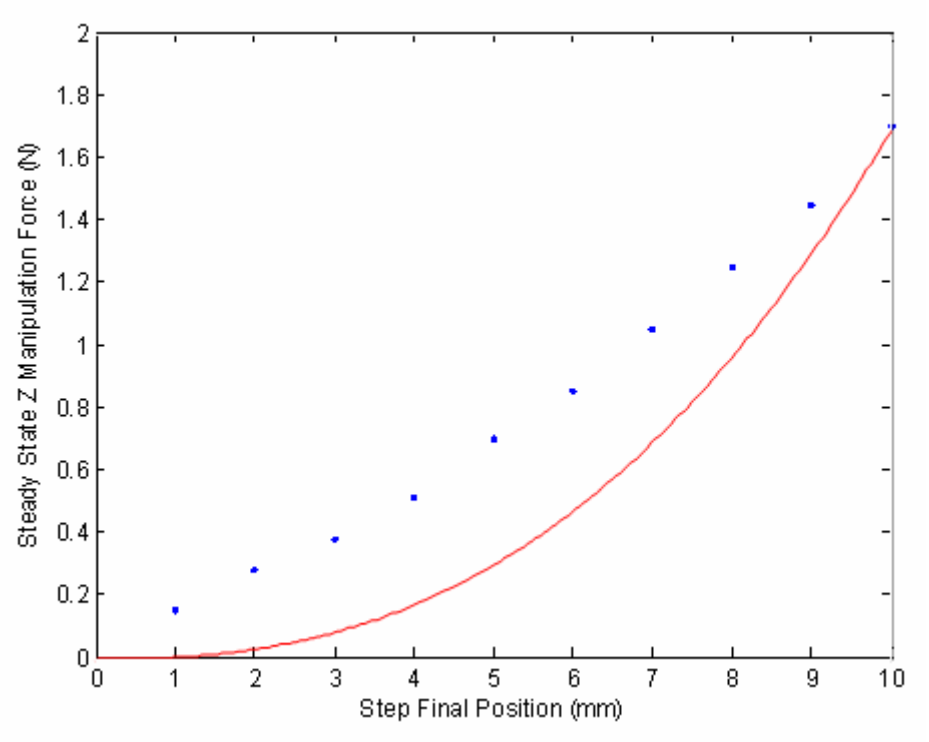


Figure 3.11: Comparison of Steady State Manipulation Forces, Pull Ramp

The error between the theoretical forces and the experimental force is due to two factors. First, variation between the anatomy of the experimental bird and the nominal bird used in the model development will cause theoretical manipulation force errors. Secondly, and more importantly, the presence of surrounding muscle tissue is not taken

into account in the model. The effect of the manipulation of muscle was assumed to be negligible in comparison to that of ligaments.

### 3.2.3 Meat Characterization

Once the error due to the displacement of the coracoid is accounted for the impact of the meat on the manipulation forces can be determined. The influence of the meat is determined by two methods here. First, a direct comparison between experimental manipulations of the same joint once with all of the meat in place around the joint and once with the meat removed, thus leaving only the ligaments to provide the manipulation force. The other method depends on modeling of the steady state manipulation force and determining the difference in steady state force from an experimental set of manipulation forces.

The difference in manipulation forces of a 10mm step pull with and without meat gives the meat characteristic for the joint given a 10mm step pull input. Figure 3.12 shows a set of experimental manipulation forces data for a 10mm step pull with and without meat on the same joint.

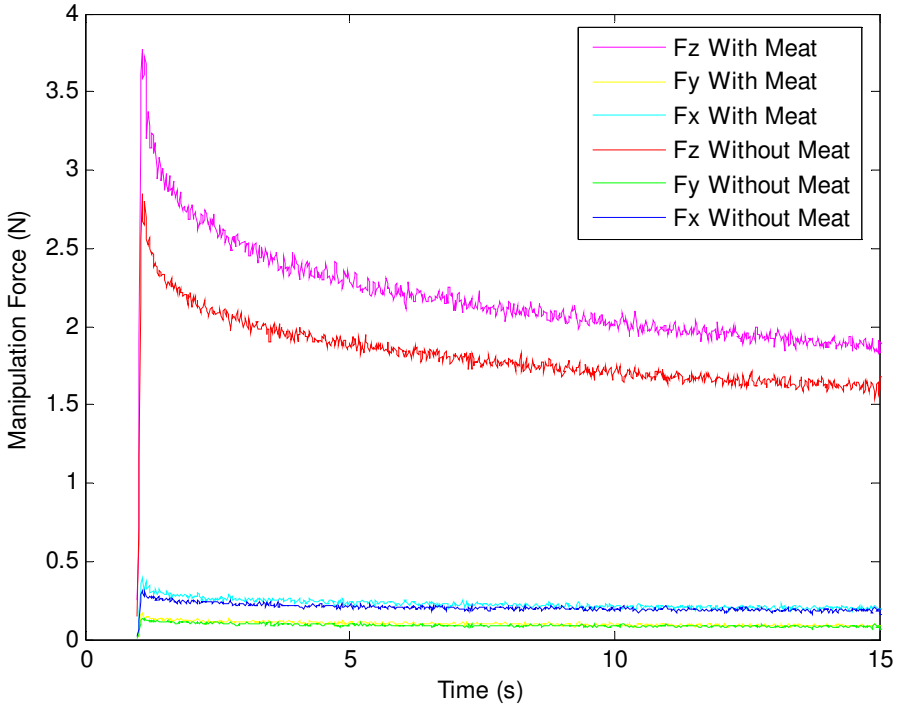


Figure 3.12: Manipulation Force With and Without Meat, 10mm Step Pull

To develop the meat characteristic for this input, the difference between $F_z$ with meat and $F_z$ without meat is developed. This difference is the effect that the meat has on the manipulation force. Figure 3.13 shows the difference in the $F_z$ forces over the entire 15 second period. It is clear that the meat has similar characteristics to that of the ligaments by comparison of the shape of the meat force characteristic to that of the ligament only manipulation. The steady state force in z-direction due to the contribution of the meat to the manipulation from experimental force comparison is 0.23 N.

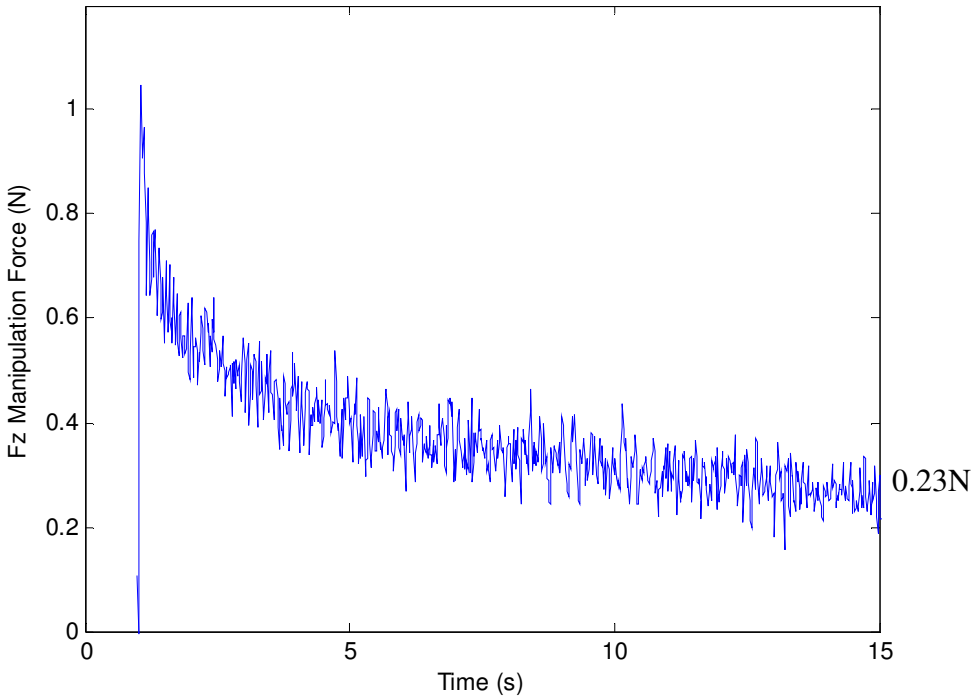


Figure 3.13: Meat Characteristic, 10mm Step Pull

Due to the limitations of the joint manipulation model, the second method does not allow for the determination of the meat characteristic during the transient, only at steady state. The steady state manipulation force for the whole joint manipulation is 1.87N. Subtracting the theoretical $F_z$ manipulation force of 1.67N, this results in a steady state $F_z$ force of 0.20N that accounts for the meat.

The steady state contributions to the $F_z$ manipulation force are approximately equal for both methods. Once the steady state meat effect is known, its influence on the manipulation can be added to the theoretical model for various inputs to produce a more accurate manipulation model.

## 3.3 Conclusions

The material characteristics developed in this chapter provide the information required for accurately applying the wing manipulation model. Section 3.1showed the experimental development of a ligament mechanics model. The stretch vs. force characteristic for a ligament was determined and normalized for application to any ligament of interest. Equation (3.1) is the characteristic equation with material dependant constants $C_o = 6.7\times10^{-4}$ and $m_o = 2.4$. The validity of this model is shown by comparison of the theoretical and experimental curve shapes.

Section 3.2applies the ligament mechanics model to the manipulation model, developed in Chapter 2, to determine the effect due to the mechanical properties of the meat on wing manipulation forces. In order to use the manipulation model to accurately predict the manipulation forces the true manipulation applied to the ligaments is determined by measurement of the body displacement under a 10mm pull manipulation. A resulting 6.3mm effective pull applied to the ligaments, as well as the nominal bird parameters shown in Table 3.2 is then applied to the manipulation model resulting in predicted steady state manipulation forces due to the ligaments. The theoretical forces are subtracted from the experimental steady state results to develop the steady state meat characteristic. For comparison purposes the meat characteristic is also developed experimentally by measurement of the manipulation force of the entire joint and subtracting the manipulation force for the same joint with all the meat removed. The resulting experimental and theoretical meat characteristics match, thus showing an effective application of the wing manipulation model in determining joint characteristics without requiring destructive exploratory procedures.

# CHAPTER 4: THE EFFECTS OF MANIPULATION ON NEEDLE PUNCTURE

## 4.1 Introduction

Procedures performed in and around joint structures during probing, and cutting operations requires high levels of accuracy in order to properly complete the task. Also of importance, the force experienced during needle insertions. This chapter discusses the experimental development of needle insertion accuracy and force improvement under manipulation, also experimental force signatures are developed for insertion into meat, ligaments, as well as hard and soft bone. Lastly, the insertion signatures are used to monitor internal structure location through measured needle insertion forces.

## 4.2 Manipulation Impact on Insertion Accuracy

This experiment is meant to quantify the accuracy improvement by means of manipulation of the wing. This is accomplished by insertion of a pin at several points defined by a grid. The intended and actual insertion locations are recorded and the location error is calculated. An improvement in accuracy will be determined by comparing the average error for insertion locations on both a free and manipulated wing.

### 4.2.1 Experimental Setup

A 3x4 grid with 5mm spacing is marked on the shoulder of both a wing under no manipulation as well as a wing under twisting and pulling manipulation. A 0.635mm (0.025 inch) diameter pin is used to puncture the shoulder at each grid point thus leaving a mark which can be located accurately using machine vision methods. An optimal grid

is overlaid on the image of the experimental grid and the distance error of each experimental point is calculated. The grid layout is shown in Figure 4.1.

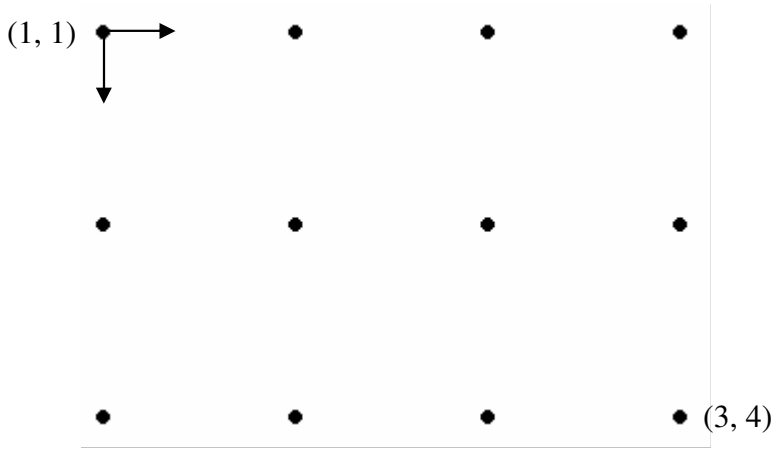

Figure 4.1: Optimal Grid

Figure 4.2 and Figure 4.3 show the experimental setup which consists of the following components:

1. A six DOF ABB robot with controller used to accurately position the marking pin. The robot location can be seen in Figure 4.2.
2. A chicken front half mounting cone. The cone is designed to rigidly constrain the chicken front half. This is accomplished by use of a prong to puncture the soft bone of the sternum, a tapered cone to fill the inside of the rib cage, and a slot where the spine placed to fix the body orientation. The cone details are shown in Figure 4.3(b and c).
3. A two DOF wing manipulator, the wing manipulator controller, force sensor, and PC. The wing manipulator is capable of providing twist and pull manipulations to the wing through a PC interface. At the interface between the manipulator and

wing is a force sensor which measures the manipulation forces. Figure 4.3 shows the location of the manipulator and surrounding cone and marking pin.

A chicken front half is placed on the mounting cone and secured solely by means of the cone geometry and gravity. For the manipulation the elbow end of the humerus is fixed to the wing manipulator in its rest position. For free wing testing the wing is left to hang freely in its rest position. The ABB six DOF robot is used to move the marking pin while placing the grid on the shoulder area. Black ink from a ball point pen is placed on the pin and is used as the marking agent on the surface of the shoulder. The area of the shoulder chosen for the grid placement encompasses soft tissue (muscle), connective tissue (ligaments and tendons), and bone. It is necessary to encounter all three materials when inserting the pin to show how contact with them may alter the pose of the free and manipulated joints.

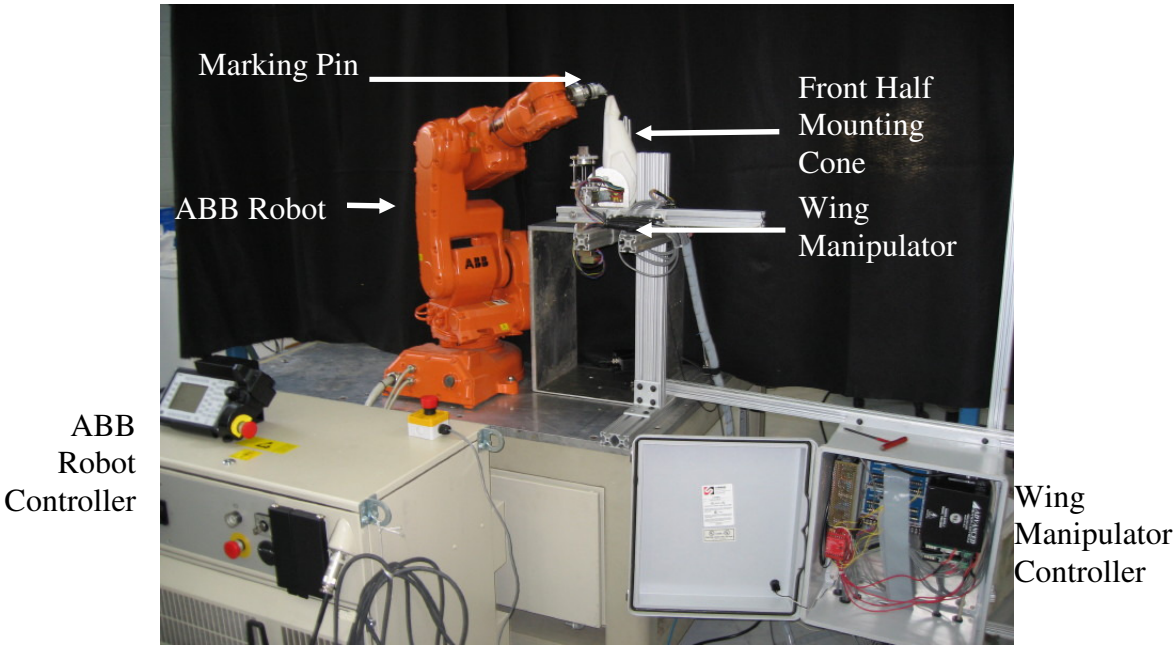


Figure 4.2: Experimental Setup

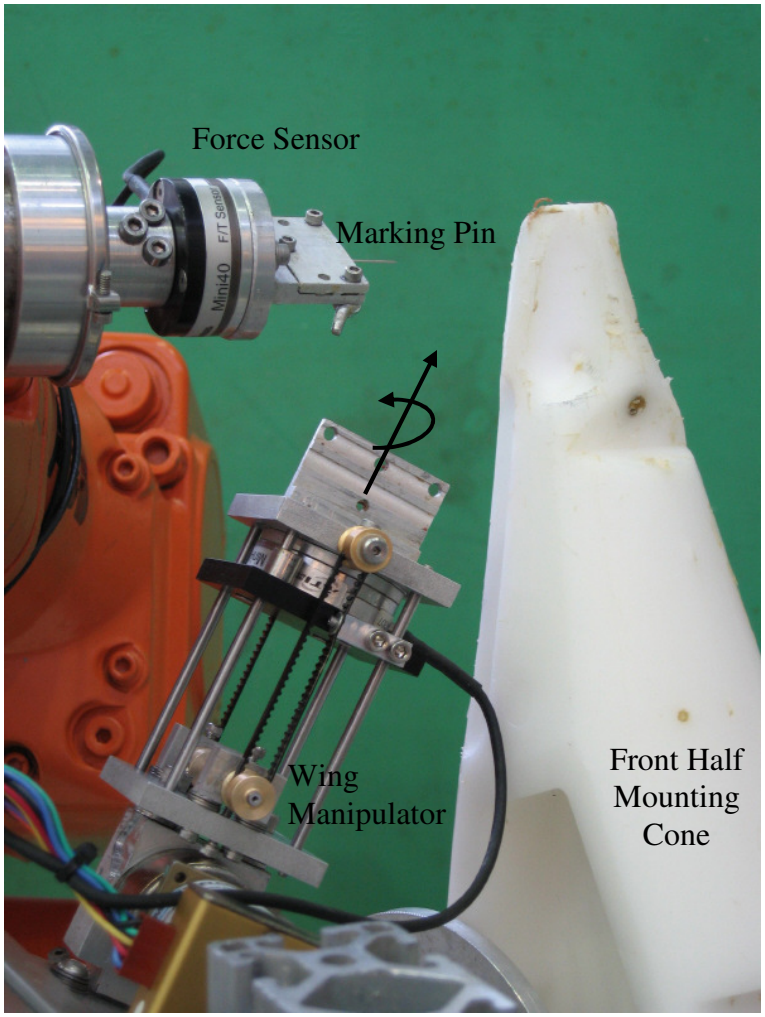


(a) Experimental Setup Detail

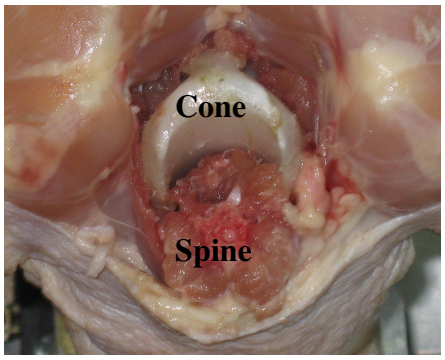


(b) Cone Detail - Top

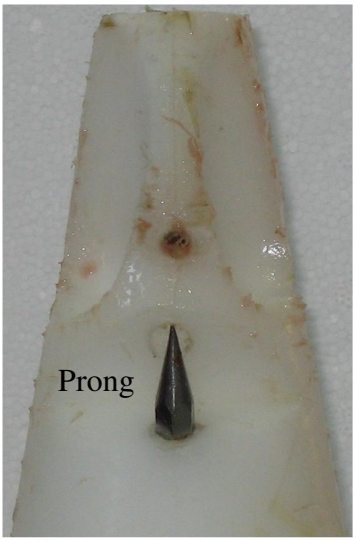


(c) Cone Detail - Front

Figure 4.3: Manipulator, Pin, and Cone Location

Once the grid has been placed, a picture is taken along the direction normal to the grid. This picture undergoes image processing to accurately determine the pin placement locations. Figure 4.4 shows a schematic of the processing used in determining the pin placement errors using image processing techniques.

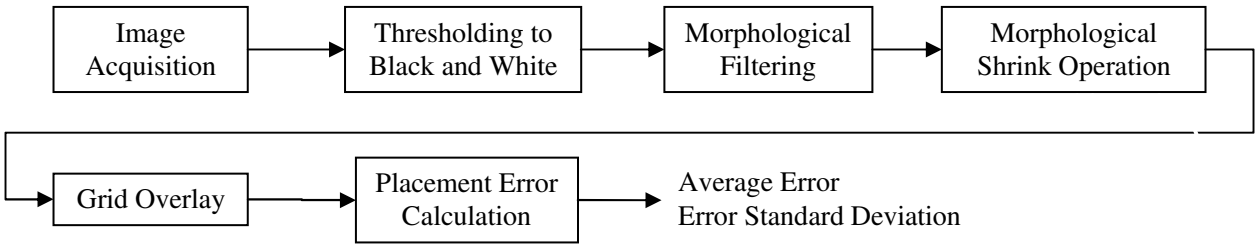


Figure 4.4: Image Processing

4.2.2 Insertion Accuracy Results

Figure 4.5 is the image of the grid marked on the free shoulder (a) and the manipulated shoulder (b). In the free wing image, the first pin placement is very small, due to the pin barley making contact with the tissue, and is located in the upper left corner of the grid. There is also a missing point at position (2,3); this is due to a lack of ink on the pin during this placement.

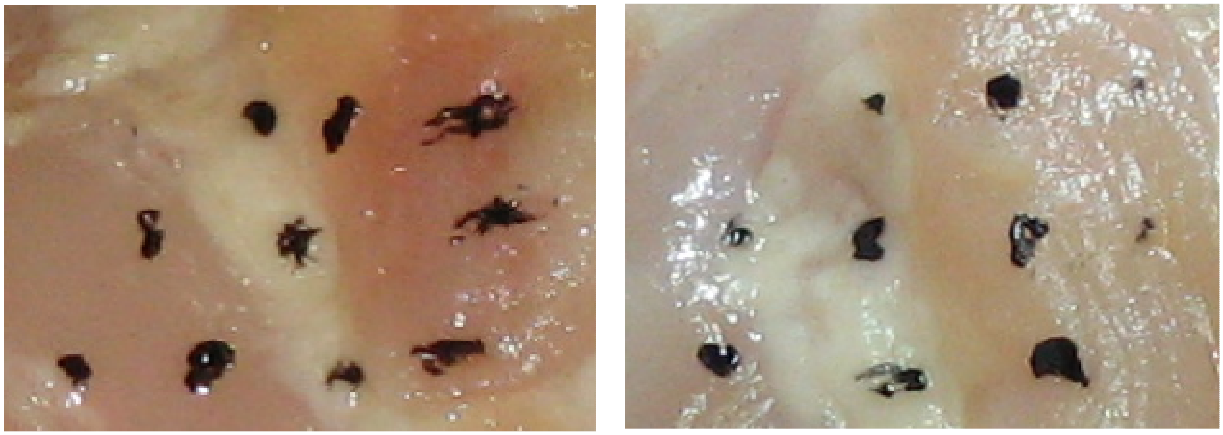

(a) Free Wing Grid (b) Manipulated Wing Grid

Figure 4.5: Actual Grid Placements

The images shown in Figure 4.5 are modified through binarization to remove the meat and leaving only the insertion locations. The application of morphological filtering and shrinking operations then shrink the insertion location marks to a single point of insertion. The actual first pin placement location is used as the reference point for the

desired grid placement, thus there will be zero error at this point. Figure 4.6 compares the location of each pin insertion (black dot) against the desired grid location (red x's).

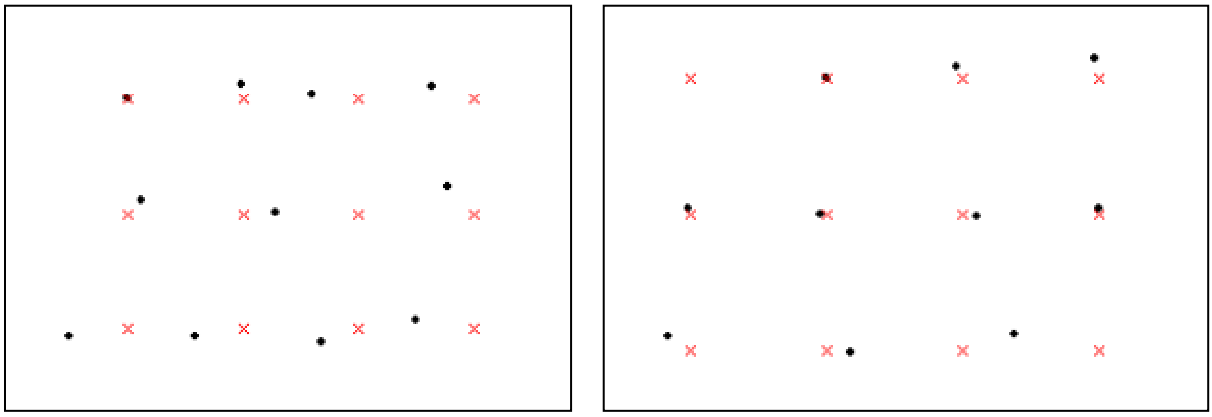

(a) Free Wing (b) Manipulated Wing

Figure 4.6: Grid Reduced to Point Locations

The pin placement errors are calculated and tabulated in Table 4.1. Also, this average placement error and error standard deviation is calculated and shown.

Table 4.1: Free Wing Grid Error Results

| **Point** | **Error (mm)** | |
|---|---|---|
| | **Free Wing** | **Manipulated Wing** |
| (1,1) | Reference | Reference |
| (1,2) | 0.61 | 0.00 |
| (1,3) | 2.01 | 0.49 |
| (1,4) | 1.86 | 0.75 |
| (2,1) | 0.83 | 0.23 |
| (2,2) | 1.44 | 0.22 |
| (2,3) | * | 0.52 |
| (2,4) | 1.60 | 0.22 |
| (3,1) | 2.46 | 0.96 |
| (3,2) | 2.07 | 0.86 |
| (3,3) | 1.68 | 2.00 |
| (3,4) | 2.50 | * |
| **Average (mm)** | **1.56** | **0.63** |
| **Standard Deviation (mm)** | **0.79** | **0.58** |

* - Not enough ink to produce visible point

## 4.3 Manipulation Effects on Insertion Forces

The forces required to perform the pin insertion or other procedures on a joint need to be minimized in order to maintain point accuracy and minimal distortion of the surrounding tissues. The effects of wing manipulation on the forces required for pin insertion is studied by recording the forces imposed on the pin by the robot while inserting it into the joint. From the pin placement accuracy test it is clear that impact with bone causes distortion but it also requires the greatest amount of force on the pin. A series of tests were run in which a pin was inserted first into breast meat, to establish a baseline force profile for insertion into soft biomaterials, then followed by insertion into the shoulder end of the humerus bone under both manipulated wing and free wing conditions. The resulting force profiles for insertion are shown in Figure 4.7, Figure 4.8, and Figure 4.10.

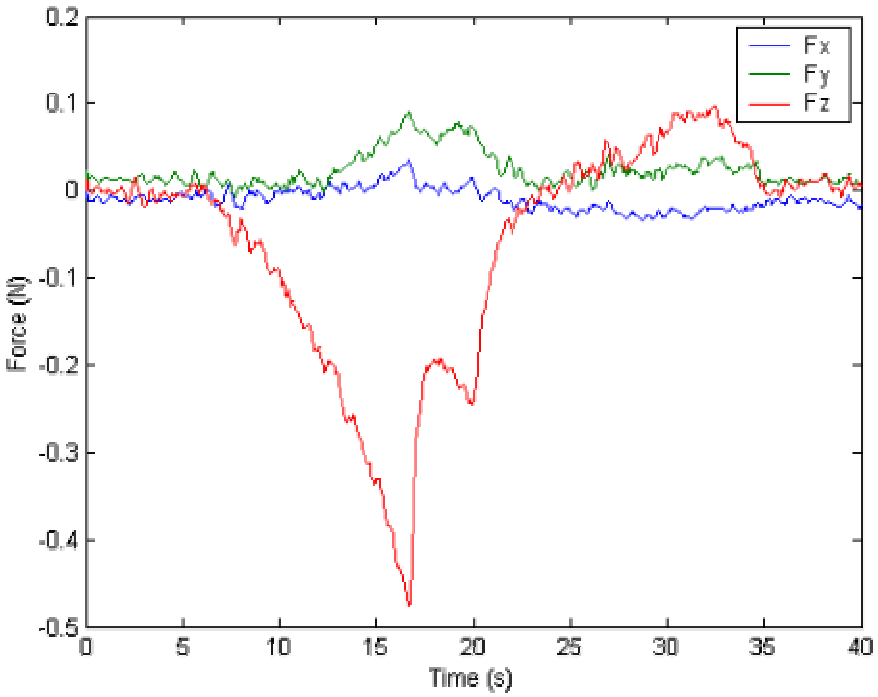


Figure 4.7: Breast Meat Pin Insertion Forces

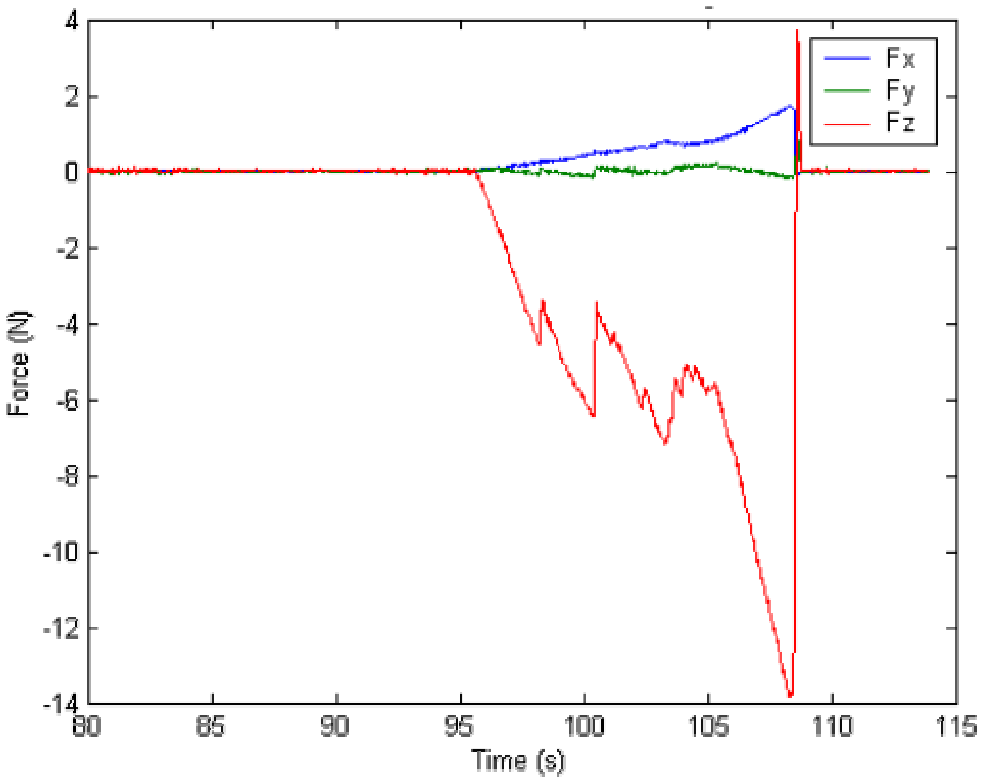


Figure 4.8: Free Bone Pin Insertion Forces

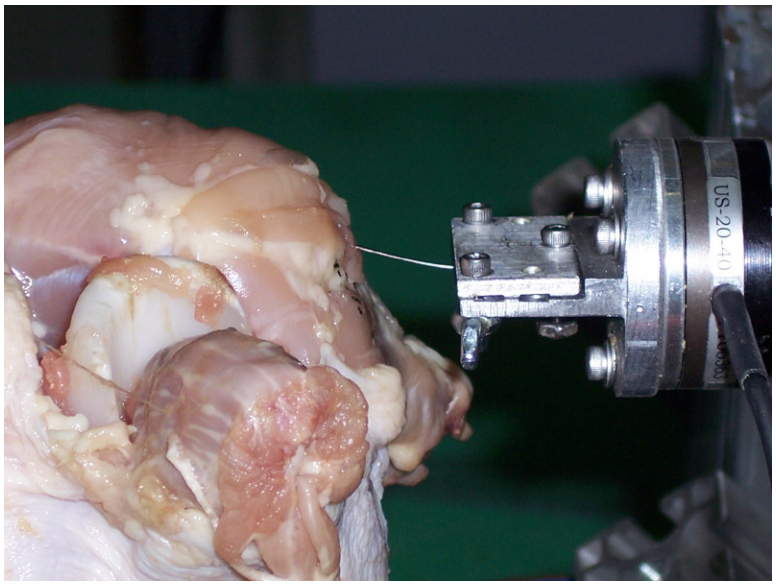

Figure 4.9: Free Wing - Pin Contact with Bone

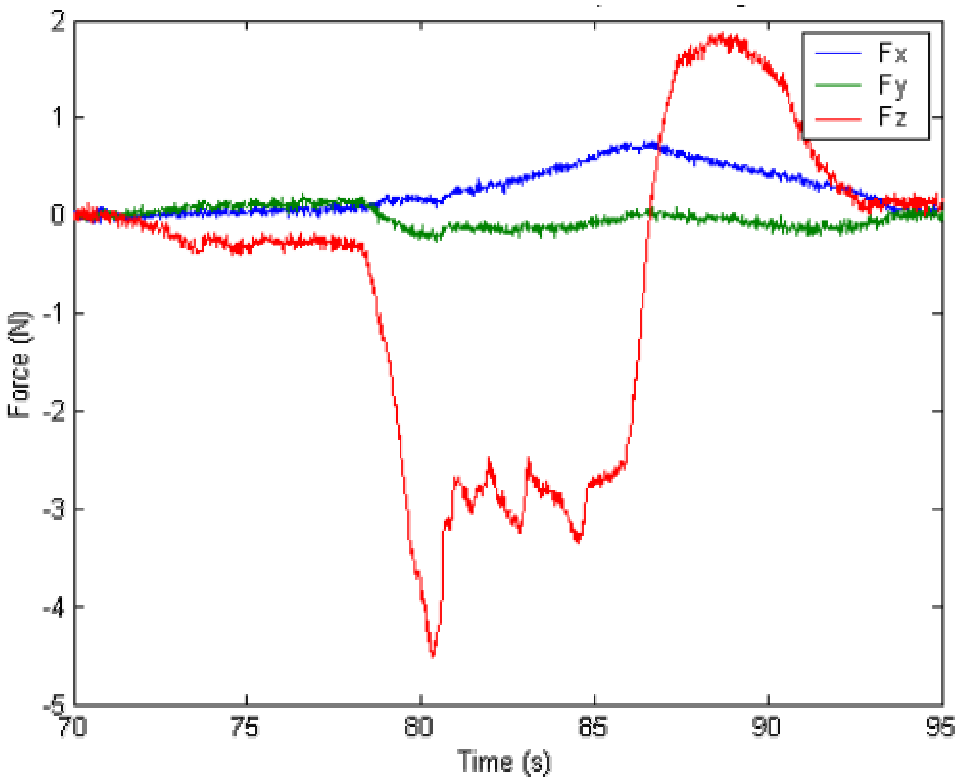


Figure 4.10: Manipulated Bone Pin Insertion Forces

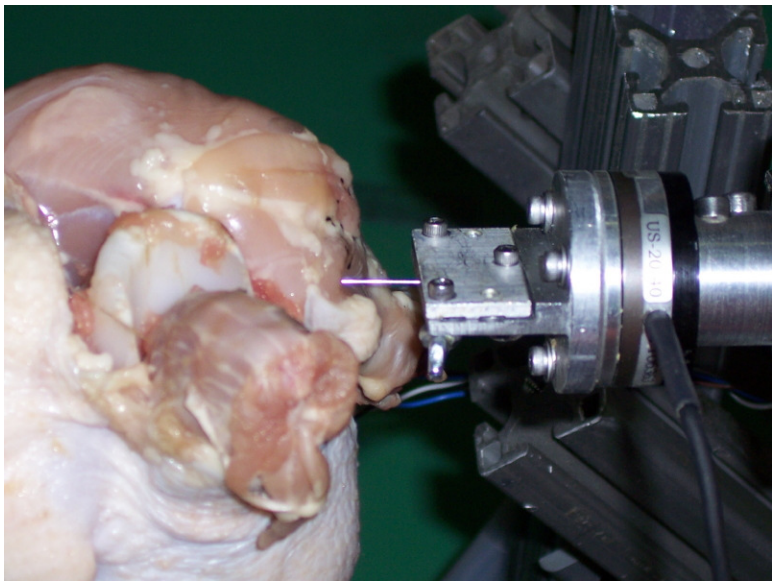

Figure 4.11: Manipulated Wing - Pin Puncture Bone

Table 4.2: Maximum Amplitude Pin Insertion Forces

| | $F_x$ (N) | $F_y$ (N) | $F_z$ (N) |
|---|---|---|---|
| **Breast Meat** | 0.1 | 0.1 | 0.5 |
| **Free -Bone** | 1.8 | 0.2 | 13.9 |
| **Manipulated - Bone** | 0.8 | 0.2 | 4.6 |

## 4.4 Insertion Force Signatures

The development of insertion force characteristic signatures for the common biological materials is performed by comparison between various samples. In this experiment the pin was used to puncture each of the biological structures, ligament, bone, meat with epimysium intact, and meat without epimysium intact, several times. The epimysium is a connective tissue membrane surrounding all internal biological structures. The following results are obtained:

- Figure 4.12 shows three experimentally developed insertion force signatures into meat with the epimysium in place.
- Figure 4.13 shows three experimentally developed insertion force signatures into meat with the Epimysium removed.
- Figure 4.14 shows three experimentally developed insertion force signatures into chicken shoulder ligaments.
- Figure 4.15 shows three experimentally developed insertion force signatures into soft bone.
- Figure 4.16 shows a comparison between each of the signatures developed above.
- Table 4.3 shows the compilation of pin insertion force signature data for the various biological materials tested above.

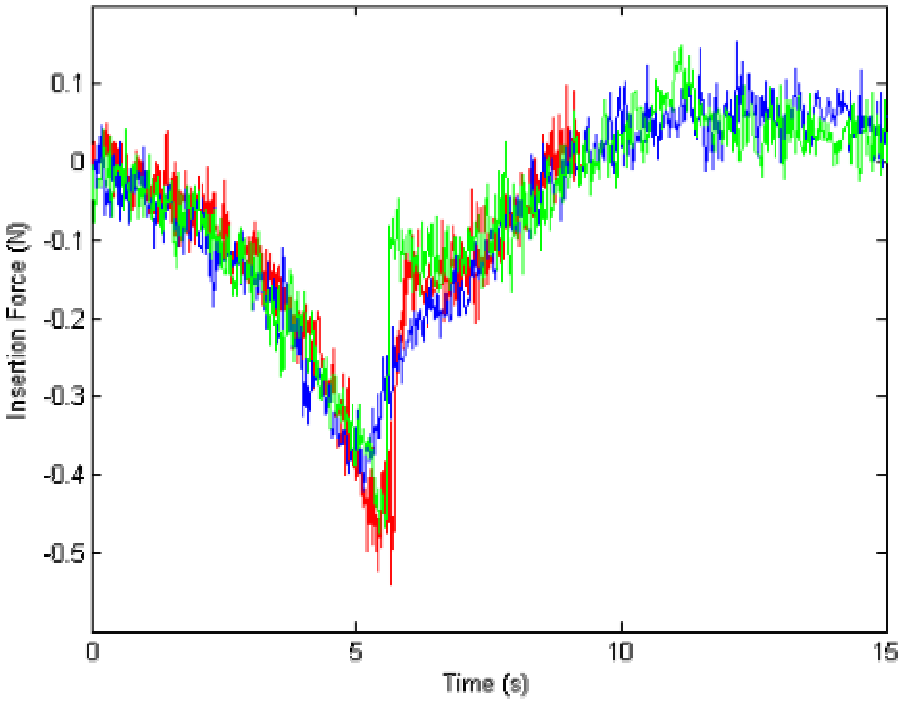


Figure 4.12: Meat with Epimysium Pin Insertion Signature

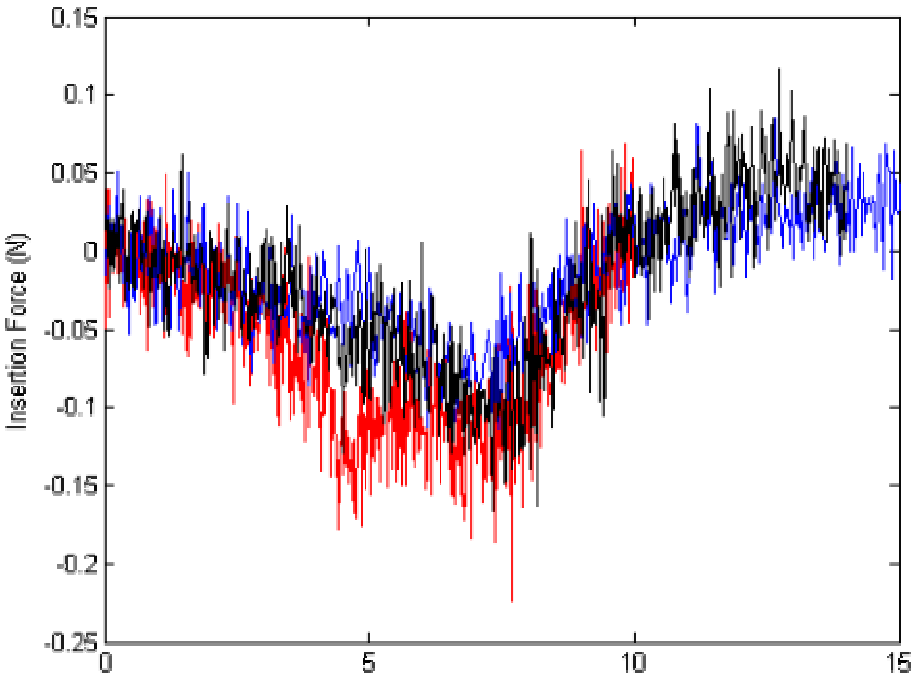


Figure 4.13: Meat without Epimysium Pin Insertion Signature

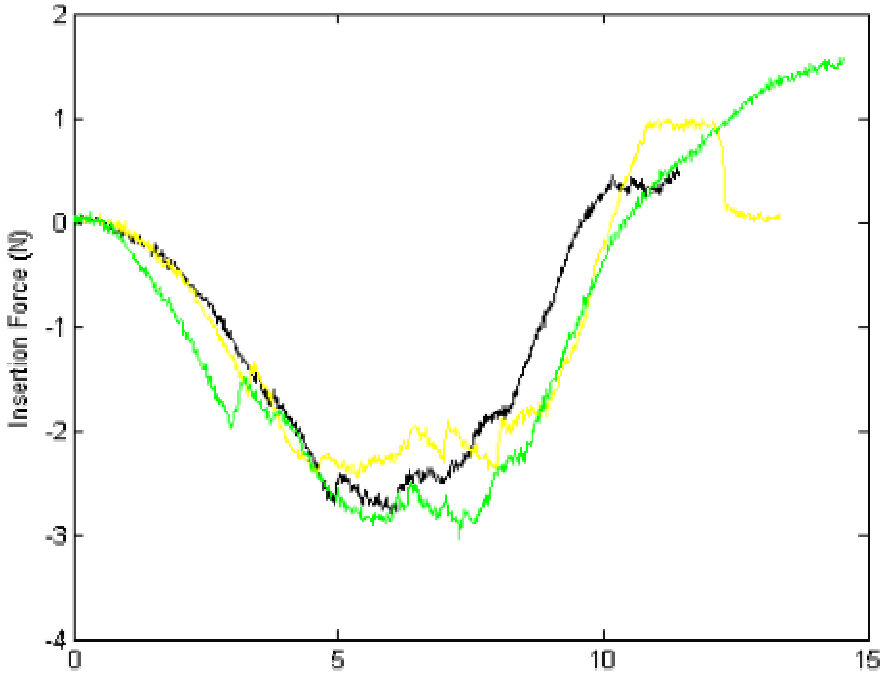


Figure 4.14: Ligament Pin Insertion Signature

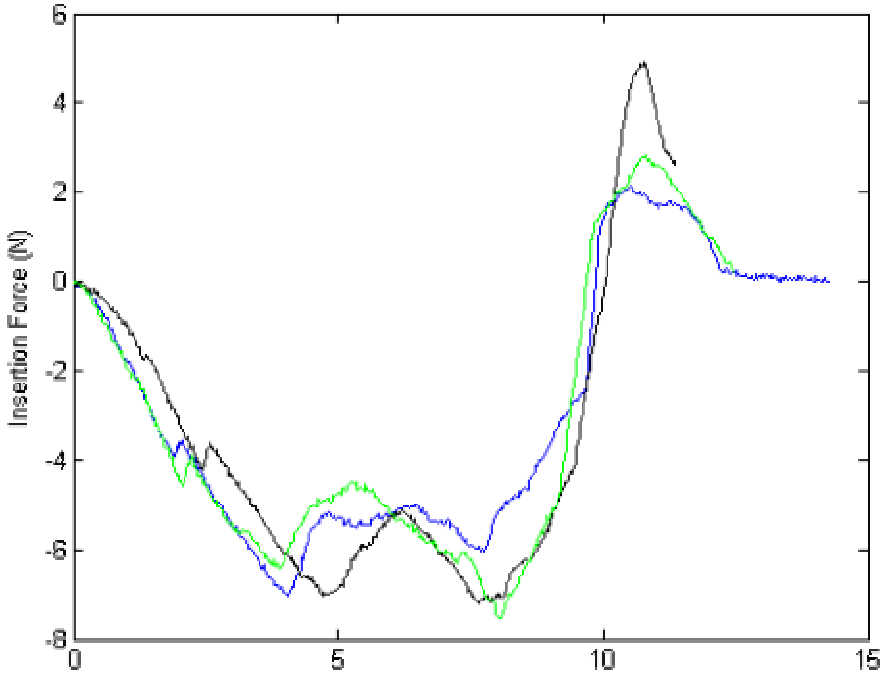


Figure 4.15: Bone Pin Insertion Signature

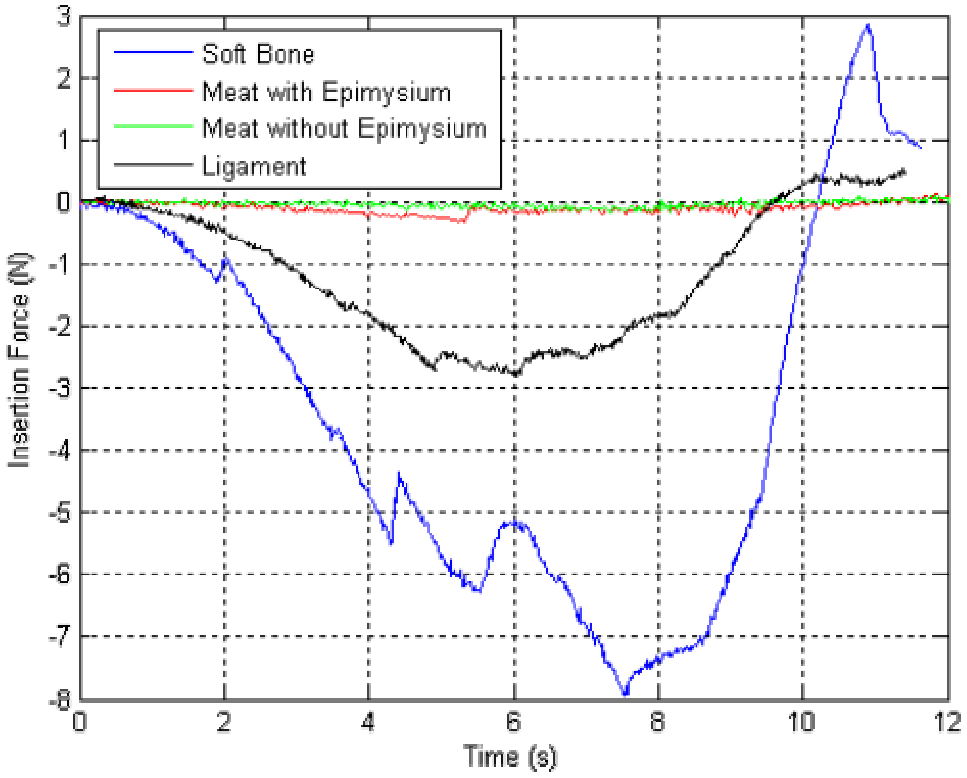


Figure 4.16: Pin Insertion Signatures

Table 4.3: Maximum Amplitude Pin Insertion Forces

| **Structure** | **Maximum Insertion Force (N)** |
|---|---|
| Meat without Epimysium | 0.13 |
| Meat with Epimysium | 0.49 |
| Ligament | 2.8 |
| Bone | 6.2 – 7.9 |

## 4.5 Internal Structure Location

Determination of the location of internal biological structures without direct observation is critical for various procedures. In the front half deboning operation the accurate location of ligaments and bones is necessary for proper cutting height location. Though noninvasive determination of the structure location is not absolutely necessary in

this application, these experimental results show the ability of force signature comparison in developing an accurate idea of the internal structure locations.

The area of interest for this thesis' application is the chicken shoulder joint; therefore, the location of ligaments and bones within the joint need to be determined. The location of the top of the humerus is crucial in the development of a proper automated cutting path. Figure 4.17 shows the pin insertion array used in determining the internal structure. The vertical array of dots is the pin insertion locations created by ink placed on the pin during testing. The first insertion point is located at 6mm below the external top of the coracoid, this point is easily located and thus is used as a reference point on all birds. The pin insertion points occur every 2mm from the first point along a vertical line that extends from the reference point down the humerus. This path passes directly over one of the major shoulder ligaments and on to the top of the humerus.

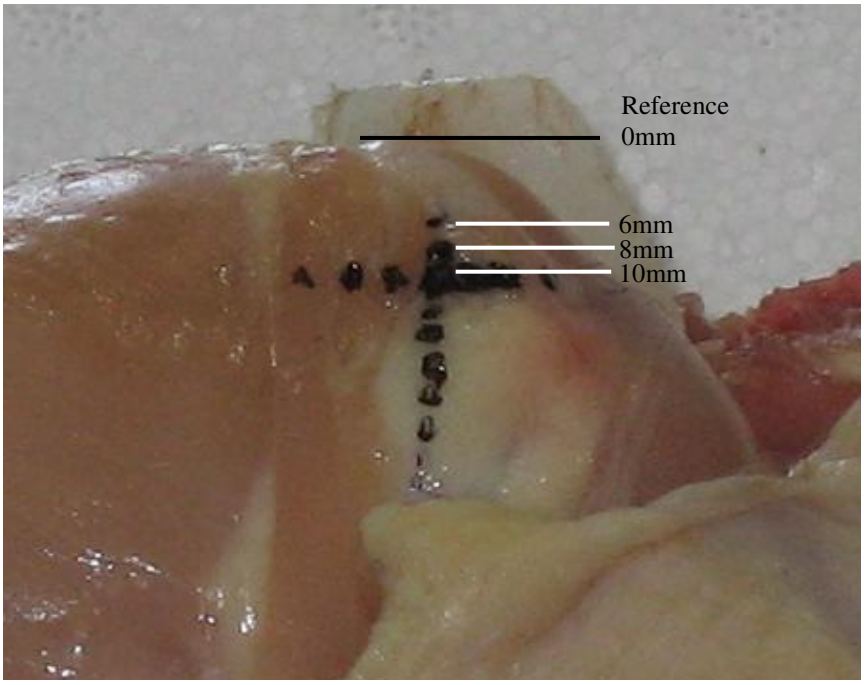


Figure 4.17: Pin Insertion Locations Down Chicken Shoulder Joint

Figure 4.18 shows the insertion forces encountered during the needle insertions shown above.

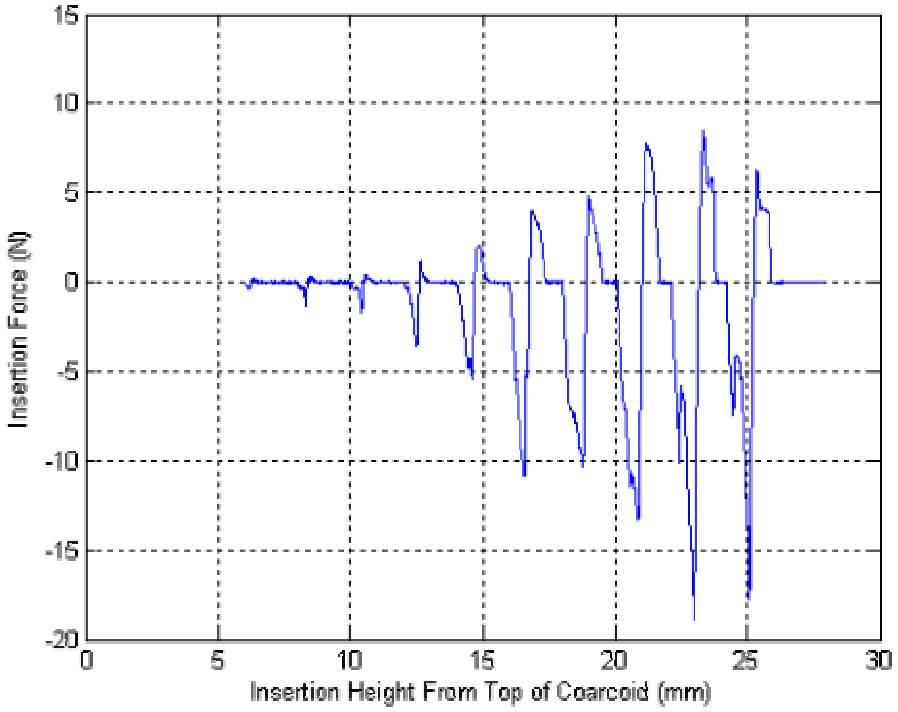


Figure 4.18: Pin Insertion Force for Vertical Array

Comparison of the insertion forces from the insertion array to the force signatures for the various biological elements that are likely to be encountered shows clearly the location of the ligament and humerus in the joint. The results from Figure 4.18 are compiled and the corresponding biological element determined in Table 4.4.

Table 4.4: Joint Internal Structure

| **Insertion Height (mm)** | **Maximum Force (N)** | **Corresponding Biological Structure – From Insertion Signatures** |
|---|---|---|
| 6 | 0.35 | Meat |
| 8 | 1.3 | Ligament |
| 10 | 1.75 | Ligament |
| 12 | 3.5 | Ligament |
| 14 | 5.4 | Soft Bone - Humerus |
| 16 … | >10.5 | Hard Bone - Humerus |

## 4.6 Discussion of Results

The two accuracy experiments show clearly the difference in accuracy provided by the free wing and the manipulated wing. The grid placed on the non-manipulated shoulder shows significant distortion as the grid placement proceeded. Figure 4.9 shows why there was such significant variation from the desired grid with the free wing. Upon contacting the bone the action of the pin is twofold, it can either bend, deflecting the bone and therefore the entire joint structure, or it can puncture the bone. In the case of the free wing, displacing the bone is easier than puncturing it and therefore the pin insertion results in significant deflection of the joint structure from its rest position. Alternately, Figure 4.11 shows the result of the pin contacting bone in the manipulated wing case. When under manipulation the position and orientation of the humerus is fixed by the manipulator on one end and the three major shoulder ligaments at the other. When under tension these ligaments provide a very stable attachment for the humerus. The result of this stability is a dramatic increase in force required to displace the bone, and therefore contact between the pin and the bone results in the pin puncturing the bone. Puncturing

the bone produces very little movement in the joint structure and therefore, the pin placement accuracy is not compromised.

The insertion force data agrees with the results from the accuracy tests and explanation. The results show that there is a clear and significant improvement of pin insertion forces using manipulation over the same insertion with no manipulation. Without wing manipulation contact between the pin and bone results in displacement of the bone, deflection of the pin, and increases the force required to insert the pin further. Manipulation of the wing provides a very stable bone structure and therefore contact between the pin and bone does not cause displacement of the bone, thus allowing the pin to penetrate the bone instead of deflecting as the bone displaces. The force required to puncture the bone and continue the insertion path results in a lower maximum insertion force.

# CHAPTER 5: APPLICATION OF WING MANIPULATION TO POULTRY CUTTING

## 5.1 Introduction

There are several cutting operations required in poultry processing. Included are cuts to separate the lower half of the bird from the upper half, leg removal from the carcass, butterfly removal from the carcass, and tenderloin removal. All of the cutting operations listed here have been automated except for the butterfly removal. This action still requires cutting by manual labor due to the complexity of the cutting path. Upon close inspection of the actions taken by the manual cutters on the processing line it has become clear that the use of wing manipulation allows for the use of a less complicated cutting trajectory and thus a more readily realizable automated cutting process.

The butterfly removal operation consists of two major cuts. The first cut, and notably the most difficult to automate, is a cut through the shoulder joint. In order to remove the butterfly the three main ligaments that provide shoulder structure must be severed. Once these ligaments have been cut, the second cut continues the incision from the back of the shoulder down through the third ligament and along the scapula bone. After the knife exits at the base of the scapula the butterfly can be removed. This is accomplished by an existing automated line which pulls on both wings thus removing the wings and breast meat from the carcass.

This chapter discusses the application of wing manipulation to the butterfly removal process. It beings with a discussion of a comparison between various cutter types and clearly provides evidence as to which will provide ease of automation,

following is an application of all the work presented in this thesis in the implementation of a the shoulder cutting operation.

## 5.2 Cutter Determination

There are several possibilities for cutters when performing poultry deboning operations. The workers use a standard paring type knife and perform a complicated but smooth slicing path through the joint. Through the use of robotics it is possible to implement different cutter types that may improve cutting efficiency or allow for more simple automation. Under consideration are three cutting schemes, straight blade cutting, circular saw cutting, and circular blade cutting.

### 5.2.1 Experimental Setup

The experimental apparatus consists of the 6 DOF ABB robot as discussed in prior sections, a chicken breast, Dremel with a 1 inch circular saw or an OLFA 28mm circular blade, and a high speed video camera. Figure 5.1(b) and (c) shows the circular cutters used in this test.

The ABB robot is used to manipulate the cutting instruments in an effort to provide constant cutting conditions to provide a basis for comparison between each cutter. The chicken breast is placed on a flat and level surface at which time the ABB robot is used to apply the cutter to the meat. Due to mounting constraints, the cutting forces for the circular saw and blade cannot be measured, therefore the performance of both of those cutters are established by analysis of the cut surface and high speed video of the cut. The mounting of the Dremel to the robot can be seen in Figure 5.1(a).

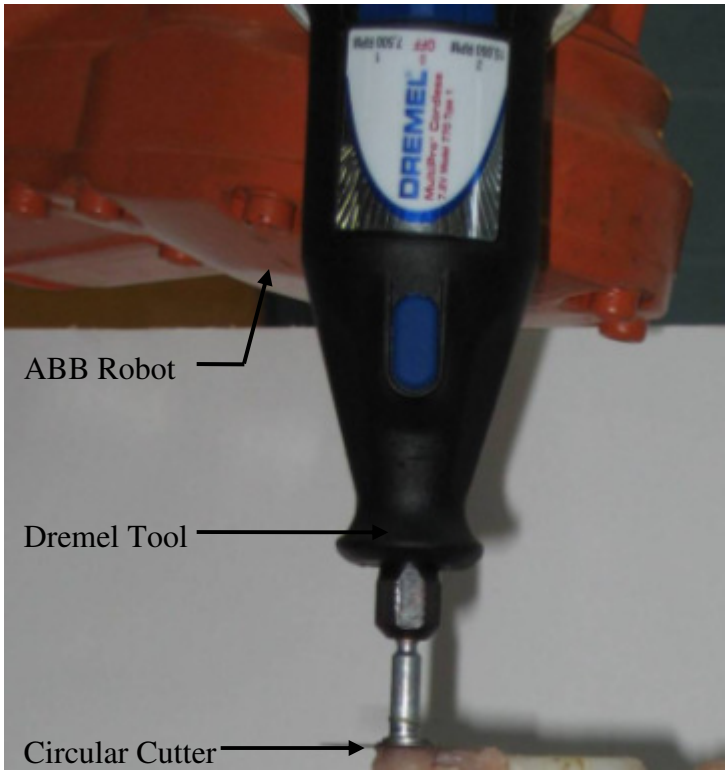


(a) Dremel Mounted to ABB Robot

(b) Circular Saw

(c) Circular Blade

Figure 5.1: Circular Cutting Apparatus

5.2.2 Cutter Determination Results

As shown through the work by Atkins and Jeronimidis [2004], the forces required for cutting of deformable materials such as biological material are greatly reduced by the presence of shearing action of the cutter. Due to this reduction in required force, it is clear that cutting with a straight blade will always require larger forces than that of both the circular saw and blade. The Dremel tool is capable of rotating the circular saw and blade at approximately 15,000 rpm. This high speed rotation produces a shearing speed at the edge of the blade of approximately 2.2 m/sec. Figure 5.2 shows the circular blade rotation and cutting velocity schematic. At this high shearing speed, even high speed translations required to maintain the desired throughput of 450 mm/sec result in a slice-

push ratio, ξ, of 49. The compressive and shearing directions are shown in Figure 5.2. Comparably, manual knife cutting generally results in a slice-push ratio of approximately 2. Application of the normalized cutting force equations (Equations 2.21 a and b) produces the cutting forces shown in Table 5.1.

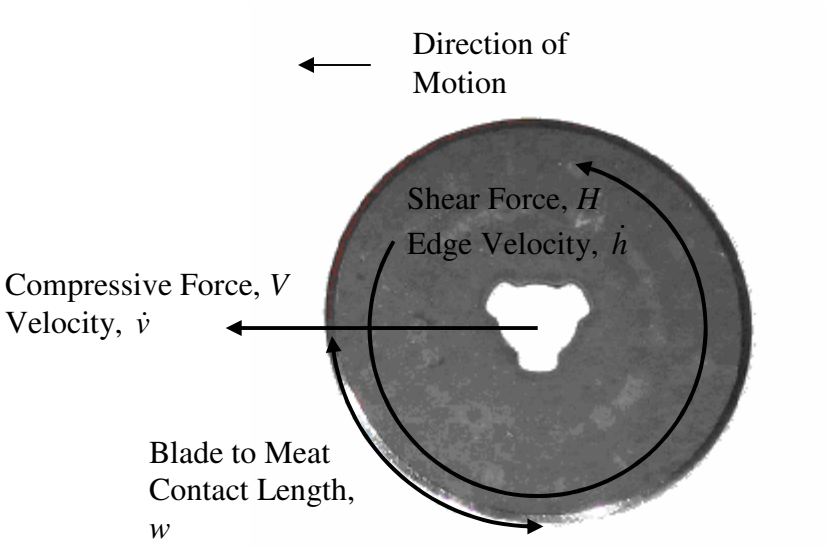


Figure 5.2: Circular Cutter Compressive and Shear Cutting

Table 5.1: Theoretical Cutting Forces

| **Normalized Cutting Forces** | **ξ=49** | **ξ=2** |
|---|---|---|
| **Shear (Horizontal)** | 0.0196 | 0.22 |
| **Compressive (Vertical)** | 0.0004 | 0.11 |

Due to the dramatic reduction in required cutting forces through use of the circular saw and blade the straight blade can be eliminated as a possible cutter for the automation of the first shoulder cut. Experimentation to determine the advantages and disadvantages between the circular saw and blade are performed and recorded by high speed video. The following Figure 5.3 (a and b) shows the cutting surface condition for cuts made with the circular saw and the circular blade respectively. Both cutters are

spinning at 15,000 rpm and translate across the breast at approximately 100 mm/sec. Figure 5.3 (a) shows the resulting surface after a cutting pass with the circular saw. Clearly visible are the rough edges and meat fragments left surrounding the edges of the incision. Figure 5.3 (b) shows the circular blade cut being clean and burr free.

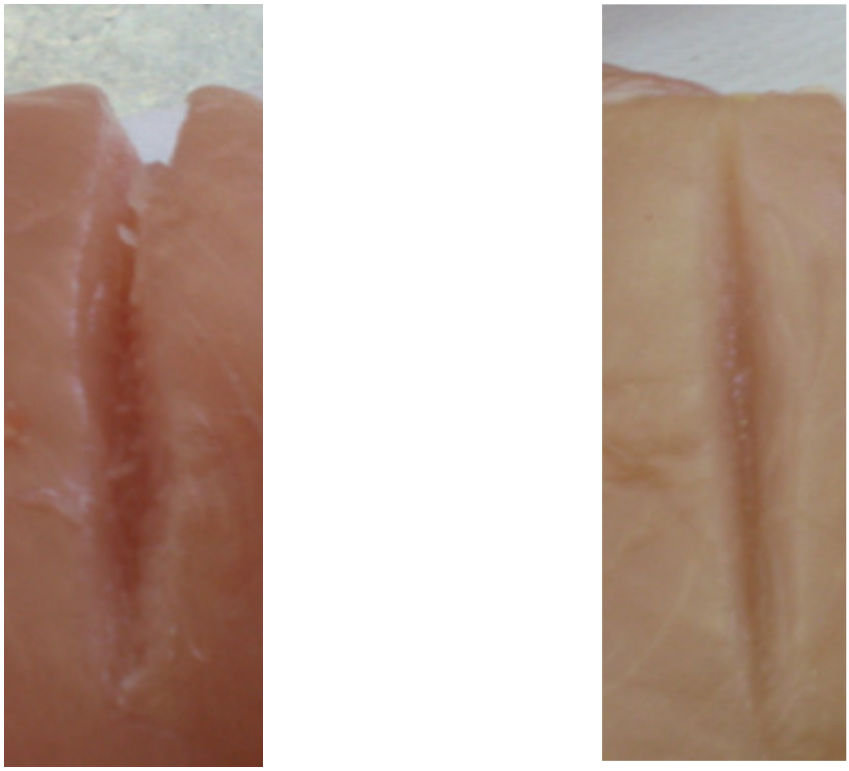

(a) Circular Saw (b) Circular Blade

Figure 5.3: Cutting Surfaces

In surgical or food processing tasks, the cut edges need to be clean and burr free in order to maintain cut integrity and presentation. Another observation made that is not depicted in either of the figure above is the consequence of the saw or blade contacting bone. Upon contact with bone the saw blade proceeds to cut away the bone material similarly to a sawing operation performed on hard engineering materials. This action results in the formation of bone chips which are deposited in the meat as the saw exits the

bone. Thus, incidental contact of the saw with bone during cutting operations will result in bone chips being left in the breast meat. Under the same circumstances, when the blade contacts the bone it does not have the same effect. The blade slices through the outermost and softest layer of the bone leaving a scored line but is unable to cut the harder interior bone. This results in the formation of no chips and also prevents the blade from fully cutting though any hard bone that it contacts.

From the evidence displayed in Figure 5.3 as well as the documented bone cutting observations, it is clear that the best cutter to use for the automation of the front half deboning operation is a circular blade similar to the one tested here.

## 5.3 Cutting Path Height Determination

Accurate determination of the cutting height which will allow for the successful completion of the joint cut is necessary. There are several methods that could be used to experimentally determine the location of the bones and ligaments in the shoulder joint. Exploration of several joints by means of tedious meat removal and measurement shows where the ligaments and bones are but has the potential of causing a loss of constraint due to the removal of the meat. This method will likely result in movement of the internal joint structure, rendering any measurements invalid. Therefore, in this thesis a method of monitoring internal structure without direct observation is used. This technique was introduced in Chapter 4 and consist of the insertion of a needle at various points around an area of interest and comparing the insertion force measured at each point to a series of force signatures. The vertical pin insertion array, first shown in Chapter 4, shows a sequence of needle insertions proceeding vertically through the shoulder joint in the direction of the humerus. The results are given in Figure 5.4 and Figure 5.1. Figure 5.4

shows the needle insertion locations beginning at 6mm below the external top of the coracoid. Figure 5.5 shows the insertion forces encountered during the needle insertions shown above.

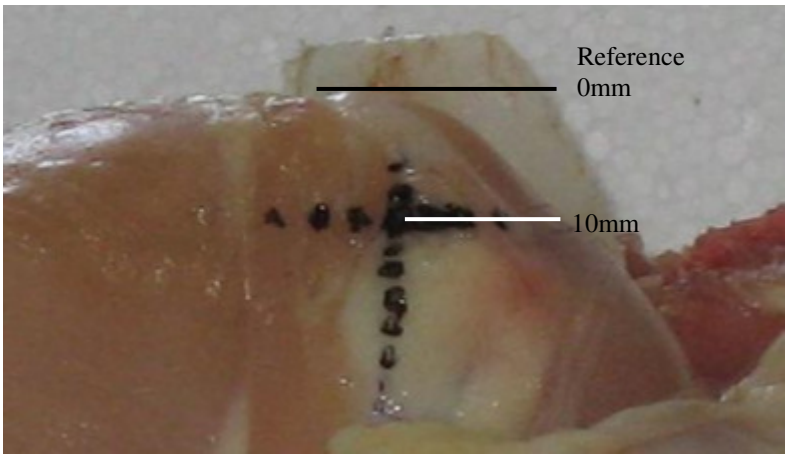


Figure 5.4: Pin Insertion Locations Down Chicken Shoulder Joint

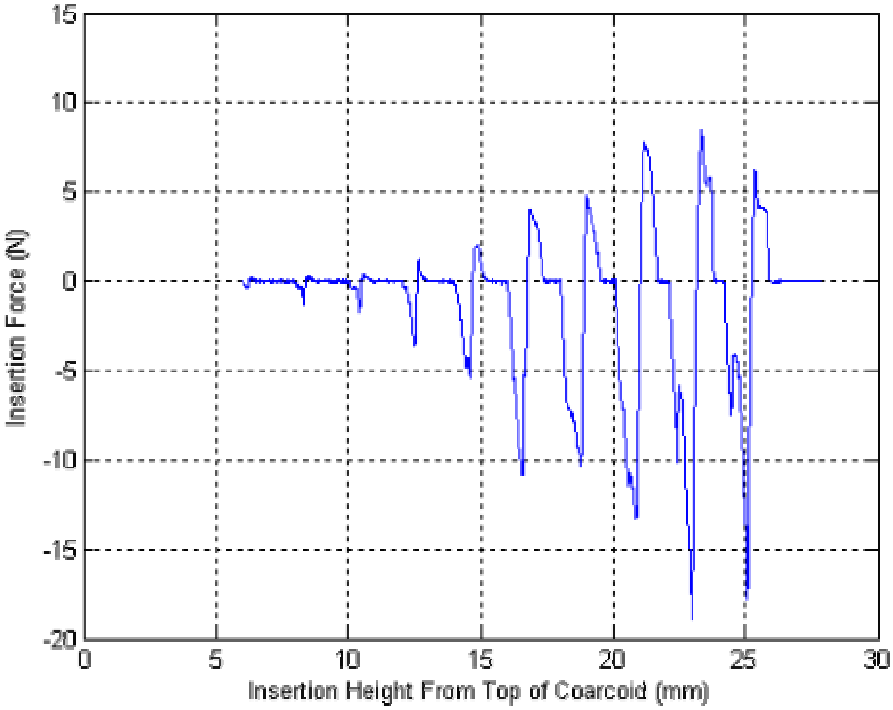


Figure 5.5: Pin Insertion Force for Vertical Array

Instead of simply monitoring the internal structure at each insertion location the determination of the cut height requires accurate locating of the top of the humerus. The very top of the humerus is soft bone and therefore will not exhibit forces as high as expected by the bone signature but it does produce a significant increase over meat or ligament insertion forces. Table 5.2 outlines the biological structure determined to be present at each insertion point.

Table 5.2: Joint Internal Structure

| **Insertion Height (mm)** | **Maximum Force (N)** | **Corresponding Biological Structure – From Insertion Signatures** |
|---|---|---|
| 6 | 0.35 | Meat |
| 8 | 1.3 | Ligament |
| 10 | 1.75 | Ligament |
| 12 | 3.5 | Ligament |
| 14 | 5.4 | Soft Bone - Humerus |
| 16 … | >10.5 | Hard Bone - Humerus |

As stated in Table 5.2 the start of the humerus occurs at 14mm below the reference point. Through knowledge of the basic joint structure as well as the desire for not cutting bone, it can be easily determined that in order to successfully cut each ligament the cutting path must be just above the humerus. Thus, a cutting path 10-12mm below the external top of the coracoid will provide the knife with the proper cutting location. Figure 5.4 also shows a horizontal pin insertion array at a height of 10mm below the reference. This series of points depicts the desired cutting path. This analysis was performed on 3 separate birds, all of which resulted in a jump in insertion force at 14mm below the reference indicating that the humerus is consistently at this location and

that the cutting path location of 10-12mm below reference will work with all birds in the nominal size range.

## 5.4 Experimental Cutting Implementation

Analysis of the process used by the manual cutters provides the basis for the cutting and manipulation trajectories used to automate the cutting process. The manual workers are presented with a bird mounted vertically on a cone. The cone is free to rotate about its central vertical axis. The worker then grabs the wing and pulls it straight down along the side of the bird, maintaining tension throughout the cut. He then places the blade horizontally at the intersection of the coracoid and clavicle and proceeds to rotate the bird so the blade of the knife remains tangent to the joint and tracks from the front, through the spread joint (due to the manipulation), and onto the back. When the tip of the knife reaches the intersection of the scapula and coracoid the worker then changes the orientation of the knife so that side of the knife is parallel to the scapula. The knife is pulled along the scapula resulting in the separation of the breast meat from the scapula. At this point the cut is complete and the same procedure is preformed on the opposite side.

In order to effectively automate this process we must understand the manual cutting path, the 'Slice and Dice' path introduced in chapter 1, and manipulations used for the first cut and further develop them into a realizable set of trajectories. To begin, the item of interest is what manipulation should be used to facilitate this cutting operation. Use of the shoulder quasi-static model can show us the forces that will be encountered by both the manipulation mechanism as well as the ligaments themselves, but it is unable to show the effects on the surrounding tissue geometry. The location and

condition of the surrounding meat is crucial to the successful automation of the shoulder cut. Therefore, it is experimentally shown that certain manipulations cause undesired positioning of the surrounding meat and therefore cannot be used.

Using the location of the circular blade as a reference, it can be clearly seen that by twisting the wing forwards or backwards results in a rising of the breast meat near the point of blade insertion. Figure 5.6 compares the resulting surrounding meat distortions due to four different manipulations performed to the wing.

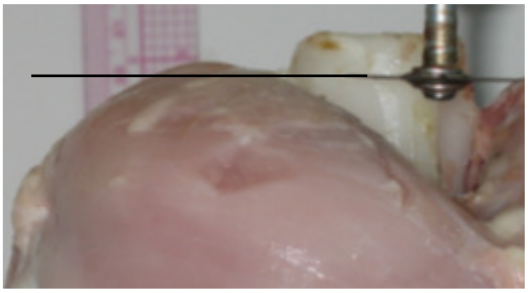

(a) Vertical Pull

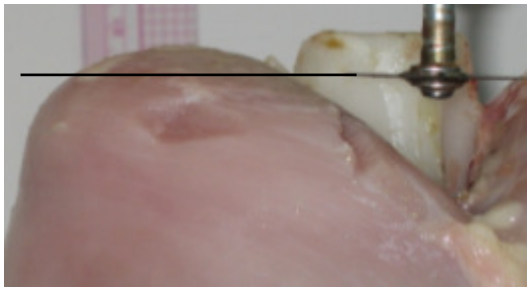

(b) Vertical Pull and Forwards Twist

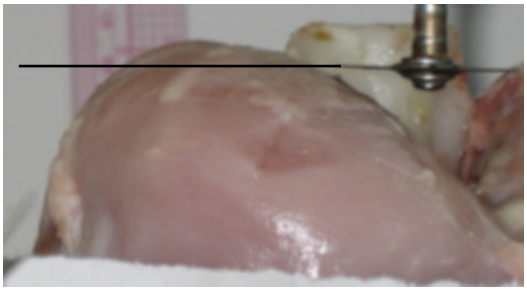

(c) Vertical Pull and Backwards Twist

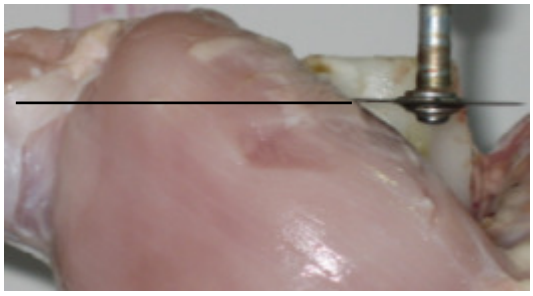

(d) Horizontal Pull

Figure 5.6: Comparison of Breast Meat Position for Various Wing Manipulations

As compared against Figure 5.6(a) manipulation of the wing in any orientation other than vertically down against the body of the bird results in significant displacement of the surrounding meat as seen in Figure 5.6 (d).

In order to minimize the amount of meat cut upon knife insertion the breast meat must be lowered. This is seen as a result of only a pull manipulation. Thus, the first step

in the wing manipulation is to apply a pull manipulation directly down the side of the carcass. Once the knife has been inserted the manipulation must be used to provide the correct shoulder pose in order to expose the ligaments to the knife along its cutting path. Continuing along the cut requires exposure of the second ligament. This ligament spans almost the entire front of the shoulder joint and therefore can be cut at almost any joint pose. Once the second ligament has been cut the constraints on the joint are significantly reduced allowing for separation of the joint. This separation will allow for the tensioning and positioning of the third ligament. This ligament is generally difficult to expose due to its near horizontal position as well as its location around the back side of the coracoid. Thus, manipulation of the wing may not present this ligament for cutting during the first cut of this operation but it does present it for easy cutting during the scapula cut.

Manipulation trajectory:

1. 10mm Pull - throughout entire first cut
2. 60 deg forward twist – to present third ligament for cutting during scapula cut

Once the manipulation trajectory is determined a comparable cutting path is developed for use with the circular blade and is shown in Figure 5.7. The cutting path is designed as follows:

1. Locate the cutting path by establishing the external top of the coracoid as a reference point for each bird.
2. Puncture, moving blade into the intersection of the clavicle and coracoid being careful not to cut the clavicle

3. Follow a circular path around the joint while also precessing about a point located directly above the joint. This results in the saw blade being at a constant angle relative to the joint.
4. Once the circular path is complete, remove the blade out the back of the bird

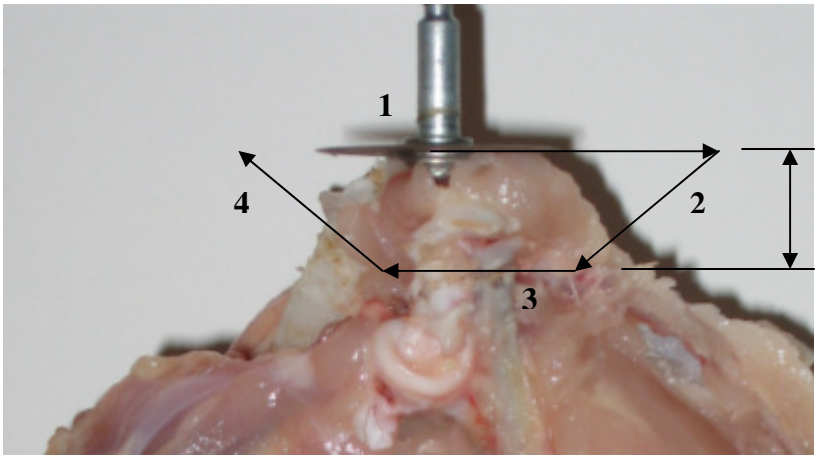

Figure 5.7: Desired Circular Blade Cutting Path

Figure 5.8 shows the orientation of the cutter during its circular path around the joint. This path is shown as segment 3 in Figure 5.7.


(a) Start of Circular Cutting Path, Side View

(b) Half Way Through Circular Path, Front View

(c) End of Circular Path, Side View

Figure 5.8: Circular Blade Orientations During Circular Cutting Path

## 5.5 Automated Cutting Results

The application of the experimentally determined information presented in this chapter culminates in the application to the automation of the front half deboning shoulder cut. The above cutting path is implemented by the ABB robot. A 28mm diameter OLFA circular blade is attached to the Dremel and rotates at 15,000rpm. In order to verify the feasibility of automating this cutting process a yield and loss comparison between a manual and automated cut is presented.

Ten birds are used in this investigation, each of which is cut using the automated path for the first cut on the right shoulder under a pulling manipulation provided by hanging a one pound weight on the wing. The automated shoulder cut is followed by the manual cutting down the scapula accompanied by twist manipulation forwards of approximately 60 degrees. The left shoulder of each bird is cut manually using the path performed by the professional cutters in the poultry processing plants. The butterfly is removed and cut in half at the breast bone seam. Each butterfly half is weighed as well as the meat left on the carcass that should have been removed along with the butterfly. Lastly, the remaining weight of the carcass is recorded. Figure 5.9 shows the butterfly after removal as well as the breast bone diving line used in cutting the butterfly halves apart.

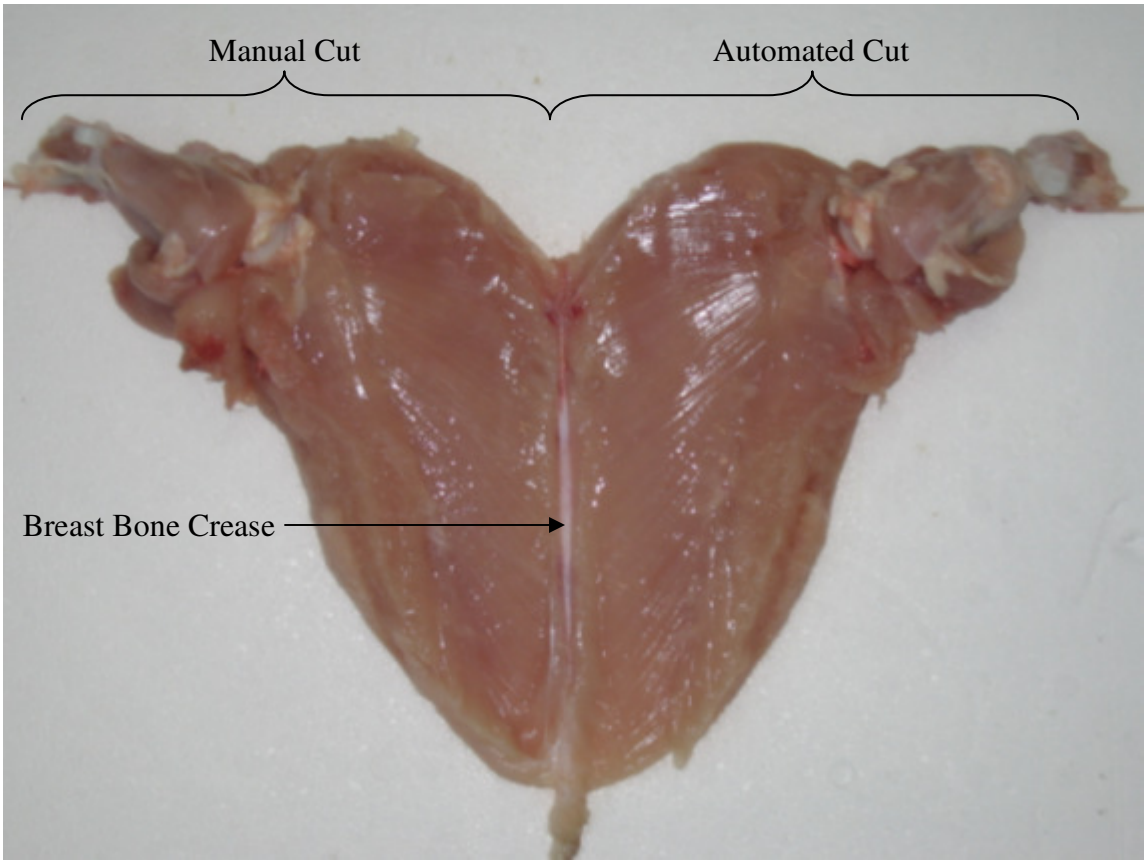

Figure 5.9: Butterfly Removed

Table 5.3 shows the raw data taken from each of the birds.

Table 5.3: Raw Yield Comparison Data

| Bird | Manual Half Butterfly (g) | Manual Scraping (g) | Automated Half Butterfly (g) | Automated Scraping (g) | Carcass (g) |
|---|---|---|---|---|---|
| 1 | 274.11 | 12.87 | 266.17 | 7.18 | 333.35 |
| 2 | 266.27 | 8.4 | 248.49 | 8.5 | 304.75 |
| 3 | 243.46 | 10.17 | 240.48 | 5.24 | 299.15 |
| 4 | 262.75 | 7.23 | 252.18 | 9.68 | 302.65 |
| 5 | 294.80 | 9.92 | 283.26 | 8.74 | 340.08 |
| 6 | 209.13 | 5.91 | 199.66 | 6.82 | 259.27 |
| 7 | 247.86 | 6.65 | 235.33 | 9.32 | 303.83 |
| 8 | 279.31 | 10.4 | 260.49 | 10.6 | 313.9 |
| 9 | 256.78 | 8.12 | 245.39 | 11.49 | 285.56 |
| 10 | 245.27 | 7.57 | 211.27 | 18.58 | 260.97 |

In order to compare the automated process to the manual process the percent yield and loss for each cut are determined. The yield and loss percentages are calculated by the following equations:

$$\text{Percent Yield} = \frac{\text{Half Butterfly}}{\frac{\text{Carcass}}{2} + \text{Scrapings} + \text{Half Butterfly}} \tag{5.1}$$

$$\text{Percent Loss} = \frac{\text{Scrapings}}{\frac{\text{Carcass}}{2} + \text{Scrapings} + \text{Half Butterfly}} \tag{5.2}$$

Table 5.4 shows the percent yield, and loss for the manual and automated cuts, as well as the different in percent yield and loss for each bird.

Table 5.4: Percentage Yield Comparison Data

| Bird | Percent Manual Yield | Percent Manual Loss | Percent Machine Yield | Percent Machine Loss | Percent Yield (Mach. – Manual) | Percent Loss (Mach. – Manual) |
|---|---|---|---|---|---|---|
| 1 | 60.42% | 2.84% | 60.49% | 1.63% | 0.07% | -1.21% |
| 2 | 62.35% | 1.97% | 60.70% | 2.08% | -1.65% | 0.11% |
| 3 | 60.38% | 2.52% | 60.84% | 1.33% | 0.45% | -1.20% |
| 4 | 62.37% | 1.72% | 61.03% | 2.34% | -1.33% | 0.63% |
| 5 | 62.09% | 2.09% | 61.31% | 1.89% | -0.79% | -0.20% |
| 6 | 60.67% | 1.71% | 59.40% | 2.03% | -1.27% | 0.31% |
| 7 | 60.99% | 1.64% | 59.34% | 2.35% | -1.64% | 0.71% |
| 8 | 62.53% | 2.33% | 60.85% | 2.49% | -1.68% | 0.16% |
| 9 | 62.99% | 1.99% | 61.69% | 2.85% | -1.30% | 0.86% |
| 10 | 63.98% | 1.97% | 58.63% | 5.16% | -5.35% | 3.18% |
| **Avg** | **61.88%** | **2.08%** | **60.43%** | **2.41%** | **-1.45%** | **0.34%** |
| **Std. Dev.** | **1.21%** | **0.38%** | **0.98%** | **1.06%** | **1.56%** | **1.23%** |

Analysis of the data presented in Table 5.4 shows clearly that in terms of yield the automated cutting path is comparable to that of manual cutting. There are several areas on the carcass where meat from the butterfly is left due to factors such as cutting path, the butterfly removal process, or previous damage to the skeletal structure. Figure 5.10 shows the common locations for meat to be left on the carcass after the deboning operation. The meat left here is considered as loss to the processing plants and every effort is made to minimize the amount of meat left on the carcass. There are three main areas at which the loss occurs. These are directly above the cutting path around the top of the coracoid, attached to the clavicle, and at the intersection of the ribcage and the tenderloin. In Figure 5.10 the areas are labeled as areas a, b, and c respectively.

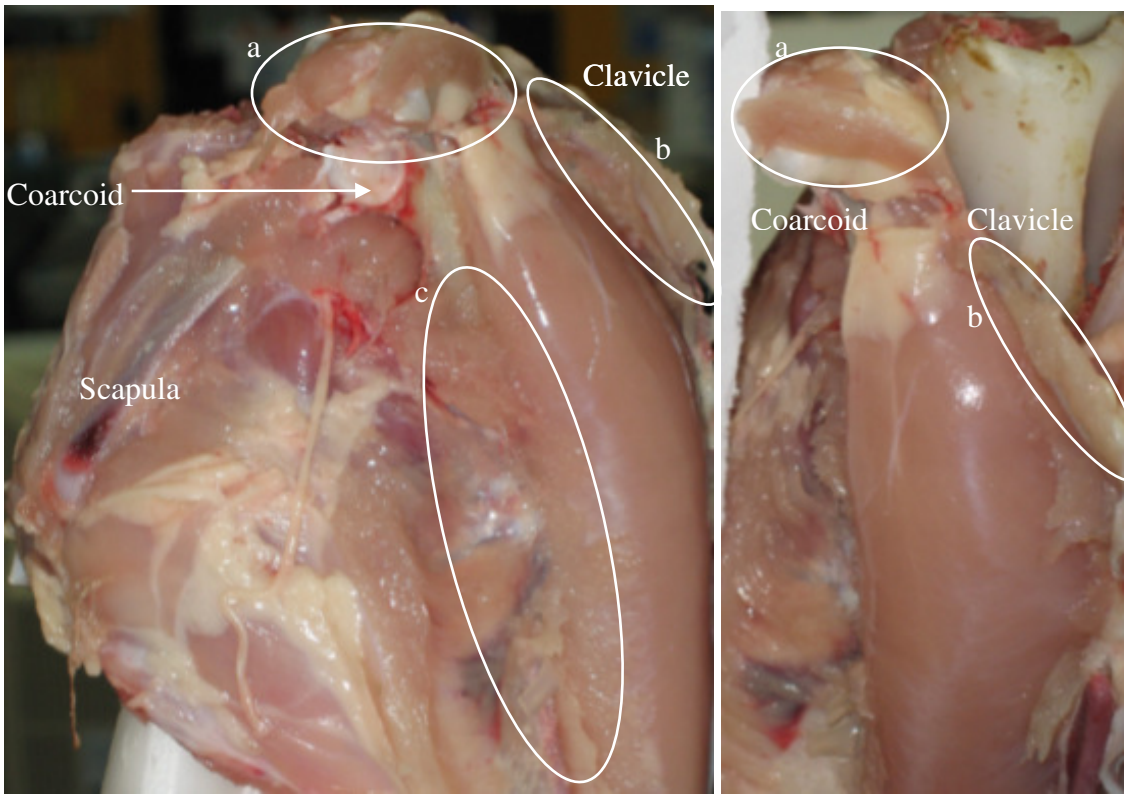


(a) Side (b) Front

Figure 5.10: Common Yield Loss Locations After Butterfly Removal

Loss in areas a, and b is due to the cutting path taken. Though loss in area "a" will always exists, it can be minimized by optimizing the cutting path as well as maintaining proper wing manipulation. Loss in area "b" is due to not cutting up to the clavicle during the initial cutter insertion. This results in connections in the meat between areas "a" and "b" and thus increases the likelihood of meat remaining along the clavicle. The loss in area "c" is not due to the cutting path or manipulation and thus cannot be controlled by wing or cutter manipulation. This loss is due to the technique used in removal of the butterfly after the cutting operations have been performed. Proper pulling angle needs to be achieved in order to minimize the loss in this area as well as other areas around the rib cage.

The ability of the prototype automated cutting path to nearly match the yield provided by manual cutting exhibits proof that the application of proper wing manipulation can facilitate the automation of the shoulder cutting operation.

Further development and refinement of the automated cutting path is expected to lead to the development of an automated cutting line capable of surpassing the manual cutter in yield, product loss, and cycle time. Improvement in each of these areas results in higher efficiency and greater throughput for the processing plant, thus overtime increasing profits and reducing or eliminating manual cutting related costs.

# CHAPTER 6: CONCLUSIONS AND FUTURE WORK

## 6.1 Conclusions

This thesis develops biological system modeling techniques capable of characterizing joint kinematics and biological material mechanics. The model development and experimentation techniques can be used as a powerful tool in the determination of proper biological material manipulation and cutting operations. Specifically, this thesis offers the following

- The quasi-static manipulation model developed in Chapter 2 successfully creates a model of manipulation forces.
- The investigation of limb manipulation in needle insertion provided very clear data supporting the benefits of manipulation in needle insertion accuracy, and needle insertion forces. Needle insertion forces are also used for determination of internal structure through the development of material specific insertion force signatures.
- The cutting study and application of manipulation to poultry processing provides clear evidence that wing manipulation can facilitate front half deboning by providing joint pose and ligament tensioning.

The ligament mechanics, joint model, and quasi-static models provide a set of tools that can be used by the food processing industry, orthopedic therapists, and surgeons alike. The nonlinear ligament mechanics and the joint kinematics model can be applied to the simulation surgical environments or other biological simulations requiring accurate joint motion. The quasi-static model can be applied when determining what

forces must be applied when placing a limb in traction or when determining what manipulation to apply when treating ligament based conditions such as frozen shoulder.

The application of biological manipulation to needle insertion tasks provides insight into a very common medical process. The process of needle insertion is used in various medical operations such as prostate brachytherapy, and medicine injections. The majority of needle insertion tasks require accurate insertion to provide proper dosage. In prostate brachytherapy an array of radioactive seeds must be placed accurately within the prostate by means of long needles. Inaccurate placement of the seeds by even a few millimeters may cause inappropriate dosage and therefore ineffective treatment of the cancer. The application of manipulation to the insertion point provides a constrained surface which prevents deformation of the material and therefore increases the accuracy of the insertion grid. Manipulation is shown to improve the average insertion point error from 1.6mm on a shoulder without manipulation to 0.59mm during manipulation. Similarly, encountering inhomogeneous materials beneath the insertion point can create needle tip deflection and increases insertion forces. The minimization of insertion force will allow for a more accurate insertion over the depth of insertion. It was shown that the application of manipulation reduced the insertion force when contact between the needle and inhomogeneous biological material occurred. The ability to determine the location of the internal structure is developed by monitoring of insertion forces and comparison to experimentally developed insertion force signatures.

Lastly, the application of manipulation to poultry procession application provided proof that manipulation of the wing and cutting device can facilitate the cutting operation while allowing for the use of a simplified cutting trajectory. Cutting with a high speed

circular blade is shown to minimize cutting forces by greatly increasing the shearing velocity and also provide a very clean cut surface. Toothed cutting devices, such as a circular saw, provide high shear speed but cause tearing of the meat at the cut surface as well as producing chips upon contact with bone that may become lodged in the breast meat. Manipulation of the wing provides joint pose to facilitate cutting by means of ligament presentation and joint separation. The cutting trajectory has been simplified to a horizontal cut with a circular blade. In order to minimize the cutting of breast meat the angle of the saw is manipulated throughout the cut while maintaining a horizontal circular path. The yield comparison provided proof that this automated cutting path produces yields comparable to that of manual cutting, and therefore further refinement of the process may lead to great product yield and consistency.

## 6.2 Future Work

The models and techniques developed in this thesis can be extended through future research. There are several areas in which the items developed for this thesis can be applied to the design of future mechanisms.

The two DOF active wing manipulator used as a test bed during the experimentation presented in this thesis provides a basis for design for a passive manipulator to be used in an automated poultry processing system.

Ligament mechanics, like all biological materials, is very complicated and thus the model developed here can be expanded to take into account the transients of the system. The force peak and relaxation cannot currently be characterized by the nonlinear spring model developed in Chapter 3. The ligament model can include the addition of a

nonlinear mass, damper, and creep can be applied to better model the transient response during manipulation.

Also, the cutting trajectory must be realized without using the six DOF ABB robot for industrial automation. The cutting path that was designed and implemented by the ABB robot includes the precession of the blade around the joint during the cut. This path can be easily realized through the use of a properly designed spherical motor. The design of the cutting system should include sensors to feedback cutting and contact forces. Implementation of force control will allow for real time modification of the cutting path thus allowing for the handling of bird size variation. The instrumented cutting tool can then be used to implement the automation of this cutting operation.

## REFERENCES


Atkins, A., Xu, X., and Jeronimidis, G. (2004). Cutting, by 'Pressing and Slicing,' of Thin Floppy Slices of Materials Illustrated by Experiments on Cheddar Cheese and Salami. Journal of Materials Science, Vol. 39, No. 8, p. 1761-2766. 15 April 2004.

Chamberlain, F. (1943). Atlas of Avian Anatomy. Michigan State College, Agricultural Experiment Station, East Lansing, MI. Hallenbeck Printing Company, Lansing, MI.

Daley, W., He, T., Lee, K-M., and Sandlin, M. (1999). Modeling of the Natural Product Deboning Process Using Biological and Human Models. IEEE/ASME International Conference on Advanced Intelligent Mechatronics, AIM, p. 49-54. 10-23 September 1999, Atlanta, GA.

DiMaio, S., and Salcudean, S. (2003). Needle Insertion Modeling and Simulation. IEEE Transactions on Robotics and Automation, Vol. 19, No. 5, p. 864-875. October 2003.

Frazzetta, T. (1988). Zoomorphology. Springer Berlin / Heidelberg. March 1988. Vol. 108, Num. 2.

Hansen, K., Weiss, J., and Barton, J. (2002). Recruitment of Tendon Crimp with Applied Tensile Strain. Transactions of the ASME Journal of Biomechanical Engineering, Vol. 124, No. 1, p. 72-77. Feb 2002.

He, T. (2000). Effects of Rotot Configurations on the Characteristic Torque of a Variable-Reluctance Spherical Motor. Doctoral Thesis in Mechanical Engineering, Georgia Institute of Technology.

Heverly, M., and Dupong, P. (2005). Trajectory Optimization for Dynamic Needle Insertion. IEEE International Conference on Robotics and Automation, p. 1646-1651. 18-22 April 2005, Barcelona, Spain.

Hing, J., Brooks, A., and Desai, J. Reality-based Estimation of Needle and Soft-tissue Interaction for Accurate Haptic Feedback in Prostate Brachytherapy Simulation. International Symposium of Robotics Research, ISRA. 12-15 October 2005, San Francisco, CA.

Hollister, S. Structure and Function of Ligaments and Tendons. Department of Biomedical Engineering, University of Michigan, BME/ME 456 Lecture Notes. http://www.engin.umich.edu/class/bme456/ligten/ligten.htm.

Holmes, J., McMurray, G., Lee, K., Zhou, D., and Claffee, M. (2005). Cut Comparison. GTRI Internal Document.

Kwon, D., Kyung, K., Kwon, S., Ra J., and Park, H. (2001) Realistic Force Reflection in a Spine Biopsy Simulator. IEEE International Conference on Robotics and Automation.

Lee, K-M. (2000). Human and Chicken Shoulder Anatomy. Georgia Institute of Technology Internal Document.

Lee, K-M. (2001). Two Cut Model. Georgia Institute of Technology Internal Document.

Lee, K-M. (2005). Verbal Discussion.

Mahvash, M. and Hayward, V. (2001). Haptic Rendering of Cutting: A Fracture Mechanics Approach. Haptics-e, The Electronic Journal of Haptics Research, Vol. 2 No. 3. 20 November 2001.

Okamura, A., Simone, S., and O'Leary, M. (2004). Force Modeling for Needle Insertion into Soft Tissue. IEEE Transactions on Biomedical Engineering, Vol. 51, No. 10, p. 1707-1716. October 2004.

Robinson, Michael C. (1970). Laboratory Anatomy of the Domestic Chicken. WM. C. Brown Company Publishers. Dubuque, Iowa.

Sandlin, M. (1998). Model-Based Vision-Guided Automated Cutting of Natural Products. Masters Thesis Mechanical Engineering, Georgia Institute of Technology.